NASA Technical Memorandum 87741

NASA-TM-87741 19860018582

MULTIAXIS AIRCRAFT CONTROL POWER FROM THRUST VECTORING AT HIGH ANGLES OF ATTACK

FRANCIS J. CAPONE AND MARY L. MASON

JUNE 1986

National Aeronautics and Space Administration

Langley Research Center
Hampton, Virginia 23665

SUMMARY

The multiaxis control power characteristics from thrust vectoring for three different fighter configurations have been determined from investigations in the Langley 16-Foot Transonic Tunnel and the Lewis 10x10-Foot Supersonic Tunnel. All three configurations employed two-dimensional convergent-divergent nozzles which provided pitch vectoring by differential deflection of the upper and lower nozzle divergent flaps. Three different means of yaw vectoring were tested: (1) a translating nozzle sidewall; (2) yaw flaps located in the nozzle sidewalls; and (3) canted nozzles. These investigations were conducted over a Mach number range of 0.15 to 2.47 at angles of attack up to 35^{o}. Nozzle pressure ratio was varied up to 28 depending upon Mach number.

The effects of pitch vectoring on the longitudinal aerodynamic characteristics followed expected trends. Pitching moment coefficient was found to vary nearly linearly with nozzle deflection angle. Similar effects on the lateral aerodynamic characteristics resulted from yaw vectoring. Both the jet-off and powered increment in either the force or moment coefficient that result from pitch or yaw vectoring remain essentially constant over the entire angle-of-attack range for all Mach numbers tested. There was no effect of pitch vectoring on the lateral aerodynamic forces and moments or of yaw vectoring on the longitudinal aerodynamic forces and moments indicating no cross-coupling of control forces and moments for combined pitch/yaw vectoring.

Longitudinal and directional control power was a function of nozzle pressure ratio and Mach number. Powered controls were very effective at low Mach numbers and their effectiveness decreased as Mach number increased due to a reduction in thrust margin. Longitudinal and directional control power from thrust vectoring was greater than that provided by aerodynamic control effects at low speeds or high angle of attack.

INTRODUCTION

The mission requirements for the next generation aircraft will dictate a highly versatile vehicle capable of operating over a wide range of flight conditions. This aircraft may have a requirement to cruise supersonically, have short take-off and landing characteristics in order to operate from bomb damaged airfields and have greater transonic and supersonic maneuverability at higher operational angles of attack than current fighters. Several studies have shown that significant advantages in air combat are gained with the ability to perform transient maneuvers at high angles of attack including brief excursions into post stall conditions (refs. 1 to 3). However, the angle-of-attack envelope of advanced fighters can be limited because of degraded stability characteristics and inadequate aerodynamic control power at high angles of attack. Providing controls that maintain high levels of effectiveness will allow future fighters to exploit a much expanded angle-of-attack envelope.

One promising method to provide large control moments that are not dependent upon angle of attack and dynamic pressure (as are aerodynamic controls) is vectoring the engine exhaust. Studies have shown that the control power provided from 10° to 15° of combined pitch/yaw vectoring can significantly enhance aircraft agility in the stall and below-stall angle-of-attack range (refs. 4 to 6). In addition, thrust vectoring provides control moments that are essentially uncoupled from airframe aerodynamics. Use of powered controls affords the aircraft designer the opportunity to reduce the size or eliminate tail and control surfaces, thereby reducing aircraft drag and weight. Because aerodynamic control surfaces are usually sized for low speed operation, they usually provide more control power than is required at high speed.

An extensive research program at the Langley Research Center has shown that thrust vectoring can be provided from multifunction (nonaxisymmetric) nozzles. Most of this research has been conducted on pitch vectoring at both static and forward flight conditions. (See for example, refs. 7 to 10.) Recent efforts have been aimed at evaluating yaw vectoring concepts at static (wind off) conditions (refs. 10 and 11). Multifunction nozzles also provide thrust reversing capability which can be used not only for STOL operation (ref. 12), but to also provide superior deceleration and closure rate for enhanced maneuverability and agility (refs. 3 and 4).

This paper presents results for three different configurations tested over a Mach number range of 0.15 to 2.47 at angles of attack up to 35°. The objective of these investigations was to determine the multiaxis control power characteristics provided by thrust vectoring. All three configurations employed two-dimensional convergent-divergent nozzles which provided pitch vectoring by differential deflection of the upper and lower nozzle divergent flaps. Three different means of yaw vectoring were tested: (1) a translating nozzle sidewall; (2) yaw flaps located in the nozzle sidewalls; and (3) canted nozzles.

SYMBOLS

All model longitudinal forces and moments are referred to the stability-axis system and all lateral forces and moments are referred to the body-axis system.

A_t nozzle throat area, $in.^2$

A_e/A_t nozzle expansion ratio (exit area ratioed to throat area)

b wing span, in.

C_L total lift coefficient including thrust component, $\frac{Lift}{qS}$

C_l total rolling moment coefficient including thrust component, $\frac{Rolling\ moment}{qSb}$

C_{l_δ} lateral control power, per degree

C_m total pitching moment coefficient including thrust component, $\frac{\text{Pitching moment}}{q S \bar{c}}$

C_{m_δ} longitudinal control power, per degree

C_n total yawing moment coefficient including thrust component, $\frac{\text{Yawing moment}}{qSb}$

C_{n_δ} directional control power, per degree

C_Y total side force coefficient including thrust component, $\frac{\text{Side force}}{qS}$

$\bar{c}$ mean geometric chord, in.

F_j measured thrust along body axis, lb

F_i ideal isentropic gross thrust, lb

F_N measured jet normal force, lb

F_r resultant gross thrust, $\sqrt{F_j^2 + F_N^2 + F_S^2}$, lb

F_S measured jet side force, lb

ℓ_j distance from c.g. to nozzle throat, in.

ℓ_t distance from c.g. to quarter chord of the horizontal or vertical tail mean geometric chord, in.

M free-stream Mach number

NPR nozzle pressure ratio

$(NPR)_{des}$ design nozzle pressure ratio

q free-stream dynamic pressure, psi

S wing reference area, $in.^2$

S_t horizontal or vertical tail area, $in.^2$

$\forall$ volume coefficient defined as follows:

horizontal tail $\frac{S_t}{S}\frac{\ell_t}{\bar{c}}$

vertical tail $\frac{S_t}{S}\frac{\ell_t}{b}$

pitch vectoring $\frac{2A_t}{S}\frac{\ell_j}{\bar{c}}$

yaw vectoring $\frac{2A_t}{S}\frac{\ell_j}{b}$

α angle of attack, deg

β angle of sideslip, deg

δ_p resultant pitch vector angle, $\tan^{-1}\frac{F_N}{F_j}$, deg

$\delta_{v,p}$ geometric pitch vector angle measured from nozzle centerline (positive for downward deflection angles), deg

for $\delta_{v,p}$ = x, left nozzle deflection = right nozzle deflection
$\delta_{v,p}$ = x/y, left nozzle deflection = x^o, right nozzle deflection = y^o
$\delta_{v,p} = \mp$, left nozzle deflection = $-x^o$, right nozzle deflection = x^o

$\delta_{v,y}$ geometric yaw vector angle (positive to left looking upstream), deg

δ_y resultant yaw vector angle, $\tan^{-1}\frac{F_S}{F_j}$, deg

θ nozzle cant angle, deg

Abbreviations:

A/B	afterburner
C-D	convergent-divergent
c.g.	center of gravity
P.S.	power setting
STOL	short take-off and landing
2-D	two-dimensional
16 FTT	Langley 16-Foot Transonic Tunnel
10x10 T	Lewis 10x10-Foot Supersonic Tunnel

APPARATUS AND PROCEDURE

These investigations were conducted in the Langley 16-Foot Transonic Tunnel (16 FTT). One of the configurations was also tested in the Lewis 10x10-Foot Supersonic Tunnel (10x10 T). The 16 FTT is a single-return, atmospheric tunnel with a slotted, octagonal test section and continuous air exchange. The wind tunnel has a variable airspeed up to a Mach number of 1.30. A complete description of this facility and its operating characteristics can be found in reference 13.

The 10x10 T is a single-return, variable-pressure tunnel with a square test section. The contour of the nozzle sidewalls is remotely adjustable and can provide a Mach number range from 2.0 to 3.5. A description of this facility can be found in reference 14.

An external high-pressure air system in each facility provided a continuous source of clean, dry air at a controlled temperature of about 90° F. This high pressure air was brought into the wind-tunnel main support system and was then passed through the various model support systems to the models. Two of the configurations were afterbody jet-effects models where the metric portion of the model on which forces and moments were measured was the afterbody. The other configuration was fully metric.

Thrust and external aerodynamic forces and moments exerted on the metric portions of each of the models were measured by an internally located six-component strain-gauge balance. Flow conditions in each nozzle were determined from measurements made from multiple total pressure and temperature probes. Sufficient pressures were measured both internally and externally to account for pressure-area and momentum tare forces acting on the models. Momentum tare forces are caused by flow transfer devices used to pass air from the nonmetric to the metric portions of the models. A complete description of these procedures are found in references 9, 13, and 15.

In each facility, multiple frames of data were averaged for each data point. Average values of the recorded data were used to compute standard force and moment coefficients based on wing area and mean geometric chord or span for reference area

and length, respectively. A complete description of the data reduction procedures for the 16 FTT is found in reference 16. Engineering units data were transmitted by telephone from the Lewis to the Langley computer complex. Final data reduction of the Lewis data were accomplished at Langley with the Langley code (ref. 15).

The adjusted longitudinal forces and moments measured by the balance were transferred from the body axis to the stability axis. Angle of attack α was obtained by applying deflection terms, caused by model support and balance bending under aerodynamic loads, and a flow angularity term to the angle of the model support system. A flow angularity adjustment of 0.1°, which is the average tunnel upflow angle measured in the Langley 16-Foot Transonic Tunnel, was applied to the 16-FTT data. No flow angularity adjustments were made for the Lewis 10x10-Foot Supersonic Tunnel.

Data were obtained in the 16 FTT at Mach numbers from 0.15 to 1.20 at angles of attack from 0° to about 35° depending on the model. Reynolds number per foot varied from 3.0×10^6 to 4.1×10^6. Data were obtained in the 10x10 T at Mach numbers from 2.00 to 2.47 at angles of attack from 0° to about 19°. Reynolds number per foot varied from 1.4×10^6 to 1.8×10^6. Nozzle pressure ratio was varied from 1 (jet-off) up to about 28 depending on Mach number. Basic data were obtained at each Mach number by varying nozzle pressure ratio at 0° or 4° angle of attack and by varying angle-of-attack at jet-off and at a fixed nozzle pressure ratio. This fixed nozzle pressure ratio represented a typical operating pressure ratio for a turbofan engine at the particular Mach number being investigated.

TWIN-ENGINE FIGHTER MODEL

Configuration 1

Model.- The twin-engine fighter afterbody model installed for testing in the 16 FTT is shown in the photograph of figure 1. The nonmetric portion of the model (not on the force balance) consisted of the forebody and the wing/centerbody sections and was supported at the wing tips in the wind tunnel. The metric portion of the model consisted of the propulsion system, afterbody shell and nozzles. The outer wing panels of the model were modified from a typical fighter wing thickness distribution to accommodate the wing-tip support system and the air supply system. The wing had an area of 644.4 $in.^2$, a 45° leading-edge sweep, an aspect ratio of 2.4, a taper ratio of 0.5, a geometric chord of 17.49 in., and a span of 40.0 in. (Table I). The wing-tip support system has the unique feature of rotating the wing with respect to the support booms. This allows testing of models to high angles of attack while keeping the model near the tunnel center line. A detailed description of the wing-tip support system is given in references 13 and 15.

A baseline two-dimensional convergent-divergent (2-D C-D) nozzle representative of an afterburning (A/B) power setting was tested on the twin-engine fighter model. Nozzle geometry included a nominal throat area of 3.9 $in.^2$, an expansion ratio of 1.24, and a design nozzle pressure ratio of 4.2. The baseline (forward-thrust) nozzle was adapted for longitudinal (pitch) thrust vectoring by differential

divergent flap deflection and for lateral (yaw) thrust vectoring by a translating sidewall concept. General sketches showing the baseline nozzle geometry with modifications for pitch and yaw thrust vectoring are given in figure 2.

The translating sidewall yaw vectoring concept consisted of truncating the right sidewall upstream of the nozzle exit and testing the nozzle with the truncated right sidewall and a full-length left sidewall. Only the right nozzle of the twin engine configuration was tested with a truncated sidewall; the left nozzle had full-length unmodified sidewalls. The length of the truncated right sidewall was set at 25 percent of the unmodified sidewall length (see fig. 2) in order to fully contain the internal flow at the nozzle throat. A more detailed discussion of the translating sidewall yaw vectoring concept is contained in reference 11.

The twin-engine fighter was also tested with a dry power nozzle configuration. This nozzle was adapted only for yaw thrust vectoring and was tested to high angles of attack.

Static performance.- Results of thrust vectoring at static conditions are summarized in figure 3 for longitudinal vectoring and in figure 4 for yaw vectoring. Static nozzle performance is presented as internal gross thrust ratio F_r/F_i, resultant pitch vector angle δ_p and resultant yaw vector angle δ_y. Neither pitch nor yaw vectoring had much effect on F_r/F_i indicating little or no losses due to flow turning. The pitch vectoring concept (differential divergent flaps) was very effective, producing resultant pitch vector angles greater than the geometric turning angle of 15^o at all nozzle pressure ratios tested. Such large pitch vector angles are typical of pitch vectoring by differential flap deflection; similar results have been reported in references 8 to 11 and 17. This concept could provide considerable longitudinal control regardless of engine operating conditions.

The yaw vectoring concept, however, produced rather small (less than 3^o) values of resultant yaw vector angles. At overexpanded nozzle operating conditions (NPR < $(NPR)_{des}$), the measured yaw vector angles were positive; at underexpanded nozzle operating conditions (NPR > 4.2) the yaw vector angles were negative. The change in the direction of the resultant yaw vector angles as nozzle operation changes from overexpanded to underexpanded indicates that the translating sidewall concept could be ineffective generating directional control at low operational pressure ratios or at transient engine operating conditions. This trend in yaw vector angle with increasing NPR was reported as a result of an earlier static study (ref. 11). However, the magnitude of the resultant yaw angles are so small (see fig. 4) that little useful directional control could be provided over the range of NPR's tested. Larger yaw vector angles at higher nozzle pressure ratios would result from translating the sidewall up to or past the nozzle throat, but such sidewall translation would probably decrease F_r/F_i (see ref. 11). In addition, increasing δ_y can also be accomplished by translation of the sidewall of the other nozzle and reducing nozzle expansion ratio A_e/A_t. These adjustments in nozzle geometry would require the addition of integrated flight and propulsion controls to the in-flight computer capabilities.

Wind-on performance.- The effects of pitch thrust vectoring on the wind-on longitudinal aerodynamic characteristics are presented in figures 5 and 6. In

figure 5, lift coefficient C_L and pitching moment coefficient C_m are presented as functions of nozzle pressure ratio for M = .60 and $\alpha = 0^o$. The increment in C_L or C_m between $\delta_{v,p} = 0^o$ and 15^o at jet-off conditions (NPR = 1.0) results from the aerodynamic flap effect of the deflected nozzle divergent flaps (see fig. 2). As nozzle pressure ratio increases, C_L increases and C_m decreases for the pitch-vectored configuration. The increase in lift coefficient with increasing NPR is due primarily to the jet lift component of the nozzle gross thrust and some jet-induced supercirculation lift. To investigate the effect of angle of attack on longitudinal control, C_m is presented as a function of α in figure 6 for M = .60 and NPR = 3.5, typical operating conditions where maneuvering capability and maximum longitudinal/lateral controls are desirable. The increment in C_m which results from pitch vectoring (increasing $\delta_{v,p}$ from 0^o to 15^o) remains constant over the entire α range tested. This result indicates that pitch thrust vectoring can provide a source of longitudinal control power which is independent of angle of attack.

The effects of yaw thrust vectoring on the lateral aerodynamic characteristics are presented in figures 7 and 8. Effects of NPR on yawing moment coefficient C_n and side force coefficient C_Y at M = .15, $\alpha = 0^o$ are shown in figure 7. The effect of α on C_n for both the dry-power nozzle and the A/B-power nozzle is shown in figure 8. The variations in wind-on lateral characteristics with NPR shown in figure 7 would be expected from the static results discussed previously (see fig. 4). At low NPR (overexpanded nozzle), yaw vectoring decreases C_n and increases C_Y; at the higher NPR (underexpanded nozzle), yaw vectoring increases C_n and decreases C_Y. Thus, as discussed earlier, yaw-vectoring by truncated sidewalls may not be feasible in producing positive yaw control over the operational NPR range without further nozzle geometry variations. As shown in figure 8, yawing moment and the increment in C_n resulting from sidewall translation were essentially independent of angle of attack. The insensitivity of the C_n increment to α is identical to the results discussed previously for pitch thrust vectoring on the longitudinal characteristics.

SUPERCRUISE MODEL

Configuration 2

Model.- Configuration 2 was a 10.5-percent scale model of a twin-engine fighter aircraft designed to cruise at supersonic speeds. The aircraft was a Mach 2.0, 49,000-pound class vehicle with a close-coupled canard and had two single-engine podded nacelles mounted under the wing that utilized multifunction 2-D C-D exhaust nozzles. The configuration was designed for self-trimming at a cruise speed of Mach 2 and a design lift coefficient of 0.10. The trim condition for the vehicle was established from the criterion that the vehicle be 5 percent unstable subsonically, which resulted in the vehicle being 4 percent stable for the supersonic design case.

A photograph showing the model mounted in the 16 FTT is presented in figure 9. The wing of this configuration had a leading edge sweep of 68^{o}, an aspect ratio of 1.53, a reference area of 936.68 $in.^{2}$, a wing mean geometric chord of 31.68 in. and a span of 37.80 in. (Table I). The 2-D C-D nozzle model geometry is presented in figure 17. This nozzle simulated an A/B power setting with a throat area of 4.90 $in.^{2}$, a throat aspect ratio of 2.84 (based on an equivalent dry power setting) and expansion ratio of 1.50, and a design nozzle pressure ratio of 6.24. A complete description of this model is found in references 9 and 18.

The model was tested with geometric pitch vector angles of 0^{o} and 15^{o}. Roll control moments were generated by differential pitch vectoring of $15^{o}/0^{o}$ with the left nozzle deflected at 15^{o} and the right at 0^{o}. The sidewalls of the nozzle were modified so that yaw vectoring flaps could be installed as shown in figure 10. This scheme is similar to the downstream flap yaw vectoring concept of reference 11 in which the flaps were installed in the nozzle sidewalls downstream of the nozzle throat. When both sidewalls are deployed, one flap deflects into the nozzle internal flow whereas the other flap deflects away from the exhaust flow. The total vectoring effectiveness of each nozzle will be realized for the current configuration because the nacelle mounted nozzles are essentially isolated from each other.

The yaw flaps were sized to operate such that there would be no interference of surfaces at both pitch vector angles of 0^{o} and 15^{o} with the flap hinge line located downstream of the rozzle throat at $\delta_{v,p} = 15^{o}$. The height of the yaw flap is then governed by its upper and lower sides remaining within the envelope formed by the upper pitch flap at $\delta_{v,p} = 15^{o}$ and lower pitch flap at $\delta_{v,p} = 0^{o}$ respectively (fig. 10). The hinge line of the flap was kept downstream of the nozzle throat in order to eliminate any thrust losses that could result from one located forward of the throat (ref. 11).

Static performance.- The resultant thrust vector angles for configuration 2 at static conditions are summarized in figure 11. The 2-D C-D nozzle exhibited excellent turning characteristics in the pitch plane. The measured value of the resultant pitch vector angle δ_{p} was greater than the geometric pitch vector angle at $\delta_{v,p} = 15^{o}$; this result is a common characteristic of resultant pitch vector angles of 2-D C-D nozzles (fig. 3 and refs. 10, 11, and 17). The thrust axis of this configuration was inclined -4.77^{o} with respect to the body axis which accounts for the level of the $\delta_{v,p} = 0^{o}$ data point and the $\delta_{p} = \delta_{v,p}$ reference line. Reference 9 also shows that the resultant pitch vector angle varies nearly linearly with the geometric pitch vector angle up to $\delta_{v,p} = 30^{o}$.

The turning characteristics in the yaw plane are shown in the center of figure 11. Since the concept of using two sidewall flaps to direct the nozzle internal flow for yaw vectoring is similar to that of pitch vectoring, the resultant yaw vector δ_{y} characteristics are also similar to pitch vector δ_{p} characteristics.

However, the resultant yaw vector angle δ_y was always smaller than the geometric yaw vector angle $\delta_{v,y}$ for all test conditions. This loss in turning effectiveness is mainly attributed to the size of the yaw flap relative to the total sidewall area. The flaps were designed to operate between pitch vector angles of 0^o and 15^o and thus utilized only a portion of the total available sidewall (fig. 10). For example, the flaps would have been about 23 percent larger if they were only required to operate at $\delta_{v,p} = 0^o$. Because these flaps do not cover the entire sidewall area, a portion of the internal exhaust flow can bypass the yaw flaps and not be turned. Similar results were obtained in reference 11. In addition, some loss in effectiveness may be caused by the cutback sidewalls (see fig. 10) which reduced the length of the flaps from that possible with full sidewalls. This probably reduces the turning capability of the left flap which was turned into the flow.

The relationship between resultant pitch and yaw thrust vector angles during simultaneous pitch and yaw vectoring operation is also shown in figure 11. There was essentially no effect of pitch vectoring on resultant yaw angle (see center plot of fig. 11). The right hand plot of figure 11 shows that, for $\delta_{v,p} = 0^o$, the resultant pitch vector angle δ_p became more negative as geometric yaw angle was varied from 0^o to -20^o whereas for $\delta_{v,p} = 15^o$, resultant pitch vector angle generally became more positive. This was especially true at NPR = 2.0 where δ_p nearly doubled as $\delta_{v,y}$ varied from 0 to -20^o. The small effects of simultaneous pitch and yaw vectoring operation on the resultant thrust vector angles suggests that there will be little or no coupling of the longitudinal and lateral control moments at forward speeds, especially for NPR > 2.0 where the interaction of simultaneous pitch and yaw vector flap inputs caused less than a 2 degree variation in δ_p or δ_y.

Wind-on performance.- Typical effects of nozzle pressure ratio on the three aircraft control moments at M = 0.60 and $\alpha = 4^o$ are shown in figure 12. Pitching moment coefficient characteristics differ somewhat from those already described for configuration 1. For this configuration, the nozzle gross thrust vector at $\delta_{v,p} = 0^o$ induces a nose-up moment because the thrust axis lies below the aircraft c.g.; at $\delta_{v,p} > 5^o$, the gross thrust axis lies above the aircraft c.g. and consequently nose-down moments will occur. However, the basic effect on pitching moment of varying pitch vector angle from 0^o to 15^o is the same as that described for configuration 1.

The variation of yawing moment coefficient with nozzle pressure ratio for three yaw vector angles (for $\delta_{v,p} = 0^o$) is shown in the center portion of figure 12. Yawing moment characteristics from vectoring are similar to pitching moment characteristics because of the similarity of the vectoring concepts. As can be seen, C_n varied nearly linearly with NPR. There was a small aerodynamic flap effect at jet-off conditions because the yaw vector flaps were relatively small. Results

which are almost identical to those shown were also obtained for a pitch vector angle of 15^{o} indicating no cross coupling of the lateral and longitudinal control moments.

The effect of nozzle pressure ratio on rolling moment coefficient is shown on the right side of figure 12. Since rolling moment was obtained by differential pitch vectoring of the left nozzle 15^{o} and the right nozzle 0^{o}, the results shown were expected. Note that rolling moment coefficient varied nearly linearly with nozzle pressure ratio. It is believed that an increment in C_{l} approximately equal to the one shown for $\delta_{v,p} = 15^{o}/0^{o}$ could be obtained by vectoring the right nozzle to a negative value (exhaust vectored up) of -15^{o}.

The effects of angle of attack on the three control moment coefficients at M = 0.60 are presented in figure 13. The increments in the moment coefficients that result from varying the respective nozzle deflection angles remain essentially constant over the entire angle-of-attack range. This result was found for this configuration over the entire Mach number range (0.20 to 2.47) tested and is identical to the results discussed for configuration 1.

The variation of the three control moment coefficients with their respective control deflection is shown in figures 14 to 16 for Mach numbers 0.20, 0.60, and 2.00. The nozzle pressure ratios noted are typical operating pressure ratios for the Mach numbers shown. In general, the control moment coefficients varied nearly linearly with control deflection. Results obtained during the investigation of reference 9 have been included in figure 14 to show pitching moment coefficient characteristics over a range of geometric pitch vector angles from 0^{o} to 30^{o}.

POWERED CONTROL ENHANCEMENT MODEL

Configuration 3

Model.- Configuration 3 was a twin-jet afterbody model in which nozzle cant angle was a test variable. Canting the nozzle was accomplished by rotating each of the nozzles about their respective thrust axis. The model with nozzle cant angles of 0^{o} and 30^{o} is shown in figure 17 and a closeup of the nozzles at a cant angle of 30^{o} is presented in figure 18. The model was also tested with a cant angle of 45^{o}. With the nozzles canted, pitching moment is obtained by symmetric nozzle pitch vectoring whereas yawing moment is produced from asymmetric nozzle pitch vectoring. An advantage of this concept is that current full-scale 2-D C-D nozzles (ref. 12) can be used without having to modify the nozzle to accommodate additional mechanisms to obtain yaw vectoring capability.

The 2-D C-D nozzle used in this investigation is shown in figure 18 at pitch vector angles of 0^{o} and 20^{o}. Pitch vector angles of 10^{o} and 30^{o} were also tested. This nozzle simulated a dry power setting with a nominal throat area of 3.50 $in.^{2}$, a throat aspection ratio of 3.5, an expansion ratio of 1.12 and a design nozzle pressure ratio of 3.23. The metric afterbody comprised the aft 36 percent of the overall model. The body lines were chosen to enclose the internal propulsion system

and fair into the afterbody enclosing the nozzles. The maximum width and height of the body were 9.00 and 5.00 in. respectively. Further details of this model are found in reference 19.

Although configuration 3 was not tested with a wing, a reference wing was assumed to nondimensionalize the force and moment coefficients. The wing reference dimensions for this configuration were based on the fact that the overall length of the body and the nozzle throat areas were sized to approximate a 10-percent scale advanced fighter aircraft. Composite dimensions for this configuration were chosen by averaging those of several fighter configurations (refs. 8, 9, 12, and 15). As a result, this model had a wing reference area of 700.00 $in.^2$, a wing mean geometric chord of 18.00 in. and a span of 40.00 in. (Table I). The c.g. was located from the nose at 69 percent of the length which is typical for fighter configurations.

Static performance.- Resultant pitch and yaw thrust vector angles are summarized in figures 20 and 21 respectively. The resultant thrust vector angles are shown as functions of geometric pitch angle $\delta_{v,p}$ and nozzle cant angle θ at a nozzle pressure ratio of 3.2 (design NPR). This nozzle exhibits the same excellent flow turning performance in the pitch plane (fig. 20) already shown for configurations 1 and 2. Because of the sizeable resultant pitch vector angles generated, measured yaw vector angles were greater than the geometric combination of $\delta_{v,p}$ and θ (fig. 21). The results presented in figures 20 and 21 show that canted nozzles can easily provide the levels of pitch and yaw vector angles that may be required for future fighters.

Wind-on performance.- The effects of pitch thrust vectoring on lift and pitching moment coefficients are summarized in figures 22 and 23. Figure 22 shows expected trends with NPR that are similar to those already described for configurations 1 and 2. As can be seen, lift coefficients measured at $\theta = 0^o$ for each of the nozzle deflections can be used to predict the resulting lift coefficients at other cant angles. The variation of pitching moment coefficient ($\delta_{v,p} = 20^o$, $\alpha = 0^o$) with nozzle cant angle for the various Mach numbers tested is presented in figure 23. Although pitching moment coefficient is shown as a function of nozzle cant angle, it actually varies linearly with the geometric function $\cos\theta$.

The effects of differential pitch thrust vectoring on the lateral aerodynamic characteristics are summarized in figures 24 and 25. The results shown in figure 24 follow expected trends. Side force coefficient can be predicted from lift coefficient measured at $\theta = 0^o$. As shown on the right side of figure 24, rolling moment is also produced by differential pitch vectoring. The rolling moment coefficient levels shown for $\delta_{v,p} = \mp 30^o$ are about the same as those produced by deflecting a rudder.

The variation of yawing moment with $\delta_{v,p}$ and θ for the various Mach numbers tested is shown in figure 25. Yawing moment coefficient varies nearly linearly with nozzle cant angle for $\delta_{v,p} = \mp 20^{o}$.

The variation of pitching and yawing moment coefficients with angle-of-attack are shown in figure 26 at M = 0.20 and NPR = 3.2. These results are similar to those already presented for configurations 1 and 2, that is, the increment in either C_m or C_n due to varying the respective deflection angle is constant oer the angle-of-attack range tested. There was no effect of sideslip on C_n over the angle-of-attack range tested as indicated by the flagged symbols. Also shown in figure 26 are the effects of a pitch/yaw combination obtained by deflecting the left nozzle 0^{o} and the right nozzle 20^{o}. This is equivalent to 10^{o} of pitch thrust vectoring to obtain pitching moment or $\mp 10^{o}$ of differential pitch thrust vectoring to obtain yawing moment. For example, the pitching moment coefficient level shown for $\delta_{v,p} = 0^{o}/20^{o}$ was essentially equal to that measured for $\delta_{v,p} = 10^{o}$ (not shown). This result again illustrates that there is generally no coupling of the longitudinal and lateral control moments when using powered controls.

COMPARISON OF POWERED AND AERODYNAMIC CONTROL POWER

An assessment of the multiaxis control power from thrust vectoring will be made by comparing control power parameters from powered and aerodynamic control effectors. The control power parameters for the powered controls were evaluated at each nozzle pressure ratio at a constant angle of attack. As noted previously, angle of attack has little or no effect on the moment increments generated by thrust deflections (powered control).

In order to facilitate the analysis of control power characteristics, a powered volume coefficient similar to the usual tail volume coefficient is defined. The horizontal tail volume coefficient is

$$\nabla = \frac{S_t}{S} \frac{\ell_t}{\bar{c}}$$

where S_t is the horizontal tail area and ℓ_t is the distance from the c.g. to the quarter chord of the tail mean geometric chord. The powered or pitch vectoring volume coefficient is defined as

$$\nabla = \frac{2A_t}{S} \frac{\ell_t}{\bar{c}}$$

where A_t is nozzle throat area and ℓ_j is the distance from the c.g. to the nozzle throat. Throat area is multiplied by a factor of 2 since all configurations reported herein were twin engine. A yaw vectoring volume coefficient is defined by replacing the mean geometric chord $\bar{c}$ with the span b.

Longitudinal control.- A comparison, at $\alpha = 0^{o}$, of longitudinal control power $C_{m_{\delta}}$ from powered and aerodynamic control effectors as a function of Mach number is presented in figure 27. Longitudinal control power from thrust vectoring was obtained for each Mach number shown at a typical operating pressure ratio (see fig. 25). Longitudinal control power available from the horizontal tail for configuration 1 (measured during tests) and from the canard of configuration 2 (ref. 18) provide a direct comparison of powered and aerodynamic controls for the same configurations. Also included in figure 27 are longitudinal control power for the F-18 (ref. 8) and F-15 (ref. 12) aircraft. Figure 27 illustrates the dependence of control power on volume coefficient; control power increases with increasing volume coefficient for both powered and aerodynamic controls.

The superiority of the powered controls over the horizontal tail for configuration 1 at low speeds is evident in figure 27. Powered controls can provide comparable control power as aerodynamic controls at low speeds. The decrease in effectiveness of the powered controls with increasing Mach number results from a decrease in available thrust margin. As can be seen, at subsonic speeds, the effectiveness of the aerodynamic controls tends to increase slightly with increasing Mach number. This result was expected since aerodynamic controls are usually sized for low speed and therefore are generally more effective than required at high speeds. Thus thrust vectoring could be used to augment the control power provided by aerodynamic controls, particularly at low speeds. As a result, the size of aerodynamic surfaces could be reduced which would reduce not only the drag of the configuration, but also the weight.

The main advantage of powered controls however will be at high angles of attack. This is illustrated in figure 28 where longitudinal control power from thrust vectoring for configurations 1 and 2 is compared to control power from both horizontal tails and canards at angles of attack up to 40^{o}. Longitudinal control power from thrust vectoring is not dependent upon angle of attack whereas control power from the aerodynamic controls decreases with increasing angle of attack. Both the horizontal tails and canards of reference 20 lost about 90% of their control power at $\alpha = 35^{o}$ to 40^{o}. In addition, reference 20 indicates that deflection of the horizontal tail was laterally stabilizing whereas canard deflection was destabilizing. This cross-coupling of the longitudinal and lateral stability or control characteristics is typical for configurations with aerodynamic controls and most likely would not occur with powered control configurations.

Directional control.- A comparison, at $\alpha = 0^{o}$, of directional control power $C_{n_{\delta}}$ from powered and aerodynamic control effectors as a function of Mach number is presented in figure 29.

Directional control power from thrust vectoring exhibits similar characteristics with Mach number as that previously noted for longitudinal control power. At low speeds ($M < 0.35$), directional control from yaw vectoring was greater than that provided by the various aerodynamic control effectors for those configurations shown. Directional control power provided by rudders was greater at Mach numbers from 0.5 to 2.0, again indicative that aerodynamic controls are usually more effective at these speeds because they are sized for low speed operation. Figure 29 also shows that yaw vectoring generally provided more directional control

than unconventional aerodynamic devices such as differential horizontal tail (ref. 21) or canard deflections (ref. 23).

The effects of angle of attack (not shown) on directional control power are also similar to those for longitudinal control power. For example, the configuration of reference 20 begins to lose directional control at about $\alpha = 20^{\circ}$ and directional control is nonexistent at about $\alpha = 45^{\circ}$. The levels of directional control power provided by yaw vectoring on the other hand will remain constant over these angles of attack.

Generally, use of a rudder for directional control will result in adverse rolling moments, that is, a positive rudder deflection causes a nose left yawing moment accompanied by positive rolling moments. These adverse rolling moments are caused because the side force generated by the rudder deflection acts above the c.g. of the aircraft. This was not the case for either configurations 2 or 3 where proverse roll resulted from yaw thrust vectoring. This occurred for configuration 2, because the nozzles were located below the c.g. of the aircraft. Thus, the vertical location of the nozzles relative to the c.g. becomes another design option for the aircraft designer. For configuration 3, proverse roll was obtained because of the anhedraled nozzles. Dihedraled nozzles would, of course, produce adverse rolling moment coupling with yawing moment.

Lateral control.- A comparison of lateral control power from differential pitch vectoring and from aerodynamic controls is presented in figure 30. As would be expected, figure 30 shows similar trends of lateral control power from thrust vectoring with Mach number as that previously discussed for both longitudinal and directional control power. The difference between the levels of lateral control power from thrust vectoring for configurations 2 and 3 results from the difference in spacing of the nozzles. Lateral control power from thrust vectoring increases with increasing nozzle spacing.

CONCLUSIONS

The multiaxis control power characteristics from thrust vectoring for three different fighter configurations over a Mach number range from 0.15 to 2.47 have been determined. The results from investigations in the Langley 16-Foot Transonic Tunnel and the Lewis 10x10-Foot Supersonic Tunnel indicate the following:

1. At static conditions, resultant pitch vector angle was always greater than the geometric pitch vector angle for the three configurations tested.

2. Positive yaw vector angles were generated at underexpanded nozzle operating conditions but negative yaw vector angles were found at overexpanded nozzle operating conditions for a nozzle using a translating sidewall to produce yaw thrust vectoring. The configuration tested was ineffective at producing yaw turning at nozzle pressure ratios typical for operation at subsonic Mach numbers.

3. Resultant yaw vector angle was always less than the geometric yaw vector angle at all test conditions for a nozzle using yaw flaps located in the nozzle sidewalls. This loss in effectiveness was

attributed to the small size of the yaw flaps relative to the total sidewall area of the nozzle.

4. Differential pitch vectoring for a canted nozzle configuration produced resultant yaw angles that were always greater than the geometric angles. This resulted from the overturning of the pitch vector angles.

5. The effects of pitch vectoring on the longitudinal aerodynamic characteristics followed expected trends. Pitching moment coefficient was found to vary nearly linearly with nozzle deflection angle. Similar effects on the lateral aerodynamic characteristics resulted from yaw vectoring.

6. Both the jet-off and powered increment in either the force or moment coefficient that resulted from pitch or yaw vectoring remain essentially constant over the entire angle-of-attack range for all Mach numbers tested.

7. There was no effect of pitch vectoring on the lateral aerodynamic forces and moments and no effect of yaw vectoring on the longitudinal aerodynamic forces and moments indicating no cross-coupling of control forces and moments for combined pitch/yaw vectoring.

8. Longitudinal and directional control power was a function of nozzle pressure ratio and Mach number. Powered controls were very effective at low Mach numbers and their effectiveness decreased as Mach number increased due to a reduction in thrust margin.

9. Longitudinal and directional control power from thrust vectoring was greater than that provided by aerodynamic control effectors at low speeds or high angles of attack.

REFERENCES

1. Herbst, W. B.: Future Fighter Technologies. AIAA Journal of Aircraft, vol. 17, no. 8, August 1980.

2. Well, K. H.; Faber, B.; and Berger, E.: Optimization of Tactical Aircraft Maneuvers Utilizing High Angles of Attack. AIAA Journal of Guidance and Control, vol. 5, no. 2, March-April 1982.

3. Skow, Andrew M.; Hamilton, William L.; and Taylor, John H.: Advanced Fighter Agility Metrics. AIAA-85-1779, August 1985.

4. Nelson, B. D.; and Nicolai, L. M.: Application of Multifunction Nozzles to Advanced Fighters. AIAA-81-2618, August 1985.

5. Pennington, Jack E.; and Meintel, Alfred J., Jr.: Performance and Human Factors Resulting from Thrust Vectoring Investigations in Simulated Air Combat. Joint Automation Control Conference, August 1980.

6. Lacey, David W.: Air Combat Advantages from Reaction Control Systems. SAE Tech. Paper Ser. 801177, October 1980.

7. Capone, Francis J.: Summary of Propulsive-Lift Research in the Langley 16-Foot Transonic Tunnel. J. Aircr., vol. 13, no. 10, October 1976, pp. 803-808.

8. Capone, Francis J.; and Berrier, Bobby L.: Investigation of Axisymmetric and Nonaxisymmetric Nozzles Installed on a 0.10-Scale F-18 Prototype Airplane Model. NASA TP-1638, 1980.

9. Capone, Francis J.; and Reubush, David E.: Effects of Varying Podded Nacelle-Nozzle Installations on Transonic Aeropropulsive Characteristics of a Supersonic Fighter Aircraft. NASA TP-2120, 1983.

10. Leavitt, Laurence D.: Summary of Nonaxisymmetric Nozzle Internal Performance from the NASA Langley Static Test Facility. AIAA-85-1347, 1985.

11. Mason, Mary L.; and Berrier, Bobby L.: Static Investigation of Several Yaw Vectoring Concepts on Nonaxisymmetric Nozzles. NASA TP-2432, 1985.

12. Mello, J. F.; and Kotansky, D. R.: Aero/Propulsion Technology for STOL and Maneuver. AIAA-85-4013, October 1985.

13. Peddrew, Kathryn H.; Compiler: A User's Guide to the Langley 16-Foot Transonic Tunnel. NASA TM-83186, 1981.

14. Aiello, Robert A.: NASA Lewis 10x10-Foot Supersonic Tunnel. NASA TM-71625, 1974.

15. Capone, Francis J.; and Mason, Mary L.: Interference Effects of Thrust Reversing on Horizontal Tail Effectiveness of a Twin-Engine Fighter Aircraft at Mach Numbers from 0.15 to 0.90. NASA TP-2350, 1984.

16. Mercer, Charles E.; Berrier, Bobby L.; Capone, Francis J.; Grayston, Alan M.; and Sherman, C. D.: Computations for the 16-Foot Transonic Tunnel - NASA Langley Research Center, NASA TM-86319, 1984.

17. Capone, Francis J.: Static Performance of Five Twin-Engine Nonaxisymmetric Nozzles with Vectoring and Reversing Capability. NASA TP-1224, 1978.

18. Capone, Francis J.; Bare, E. Ann; and Arbiter, Dorothy G.: Aerodynamic Characteristics of a Supersonic Fighter Model at Mach 0.60 to 2.47. NASA TP-2580, 1986.

19. Mason, Mary L.; and Capone, Francis J.: Aeropropulsive Characteristics of Twin Single-Expansion-Ramp Vectoring Nozzles Installed with Forward-Swept Wings and Canards. NASA TP-2133, 1983.

20. Klein, John R.; Walck, Kenneth J.; and Hahne, David E.: Airframe Component Effects on the Aerodynamic Stability and Control Characteristics of a Supersonic Cruise Fighter at High Angles of Attack. AIAA-84-2110, August 1984.

21. Lallman, Frederick J.: Preliminary Design Study of a Lateral-Directional Control System Using Thrust Vectoring. NASA TM-86425, 1985.

22. White, S. N.: Feasibility Study for Integrating Thrust Vectoring as a Primary Flight Control System. NASA CR-165758, 1981.

23. Re, Richard J.; and Capone, Francis J.: An Investigation of a Close-Coupled Canard as a Direct Side-Force Generator on a Fighter Model at Mach Numbers From 0.40 to 0.90. NASA TN D-8510, 1977.

TABLE I.- MODEL REFERENCE DIMENSIONS AND TEST CONDITIONS

	Configuration		
	1	2	3
S, in^2	644.40	936.68	700.00
$\bar{c}$, in	17.49	31.68	18.00
b, in	40.00	37.80	40.00
P.S.	Dry : A/B	A/B	Dry
A_t, in^2	2.71 : 3.9	4.9	3.5
A_e/A_t	1.15 : 1.24	1.50	1.12
$(NPR)_{des}$	3.50 : 4.20	6.24	3.23
M_{range}	0.15 → 1.20	0.20 → 2.47	0.20 → 1.20
α_{range}	0 → 36°	0 → 20°	0 → 27°

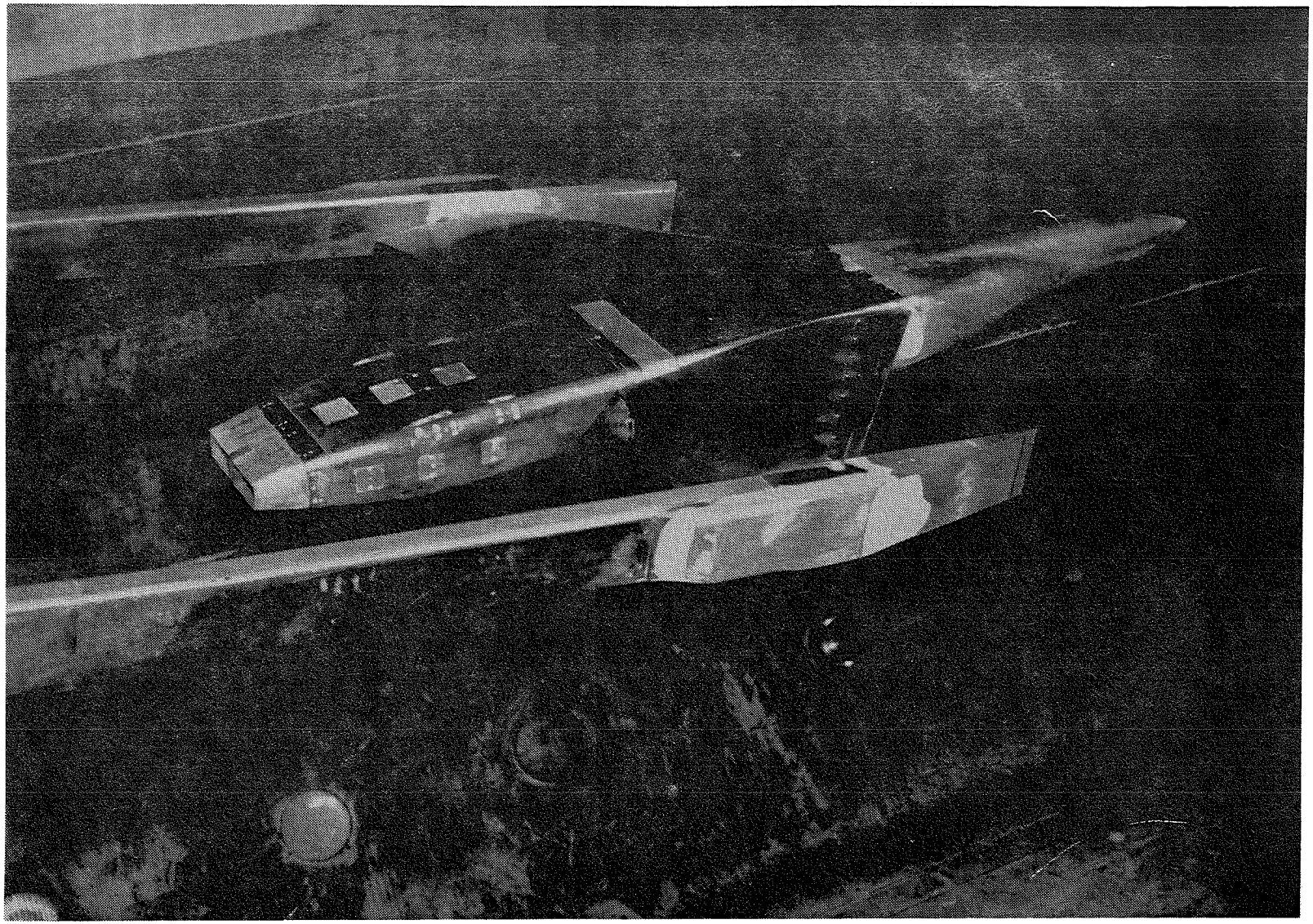

Figure 1.- Configuration 1, twin-engine fighter model.

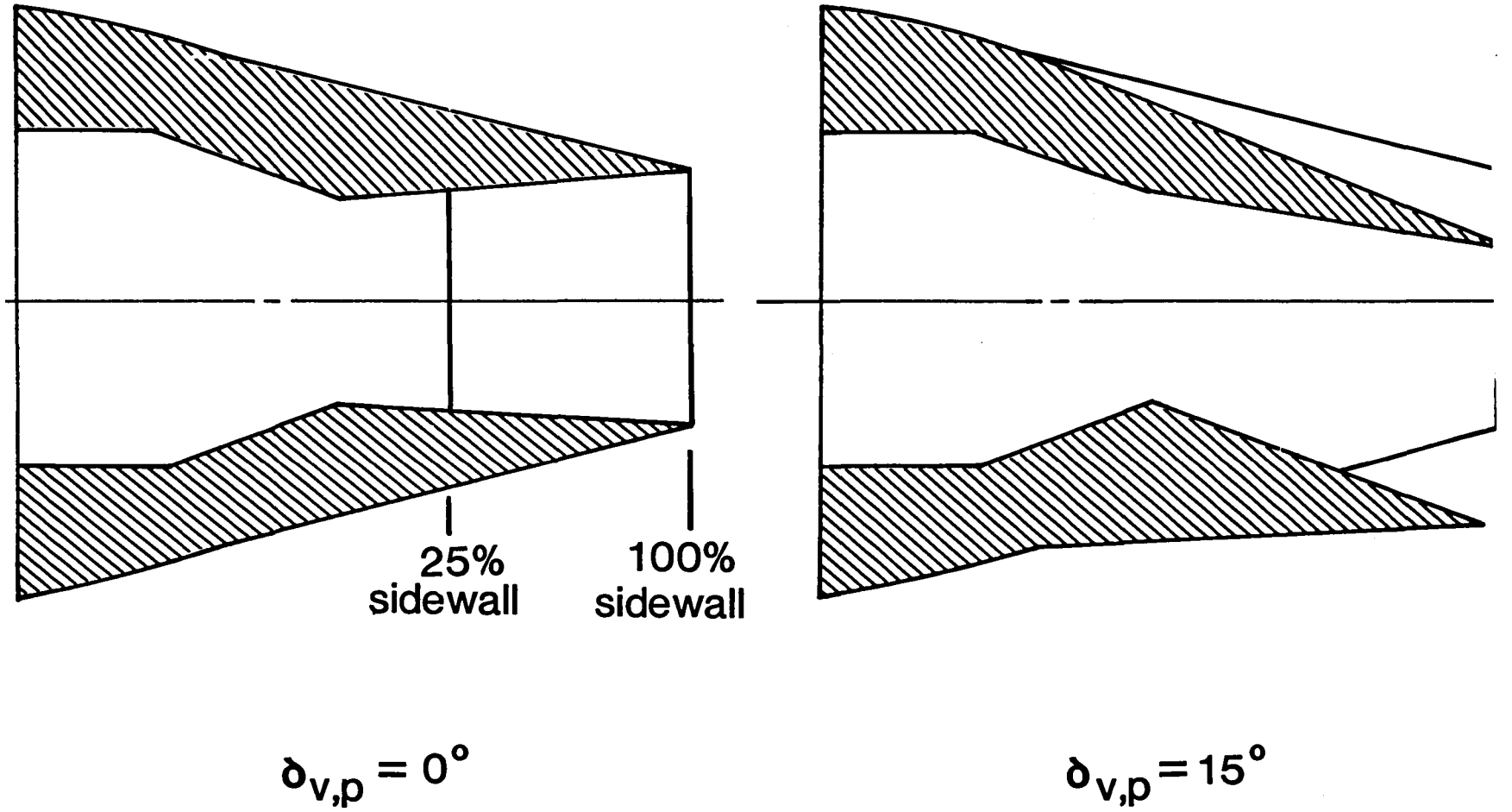

Figure 2.- Configuration 1, 2-D C-D nozzle geometry, A/B power.

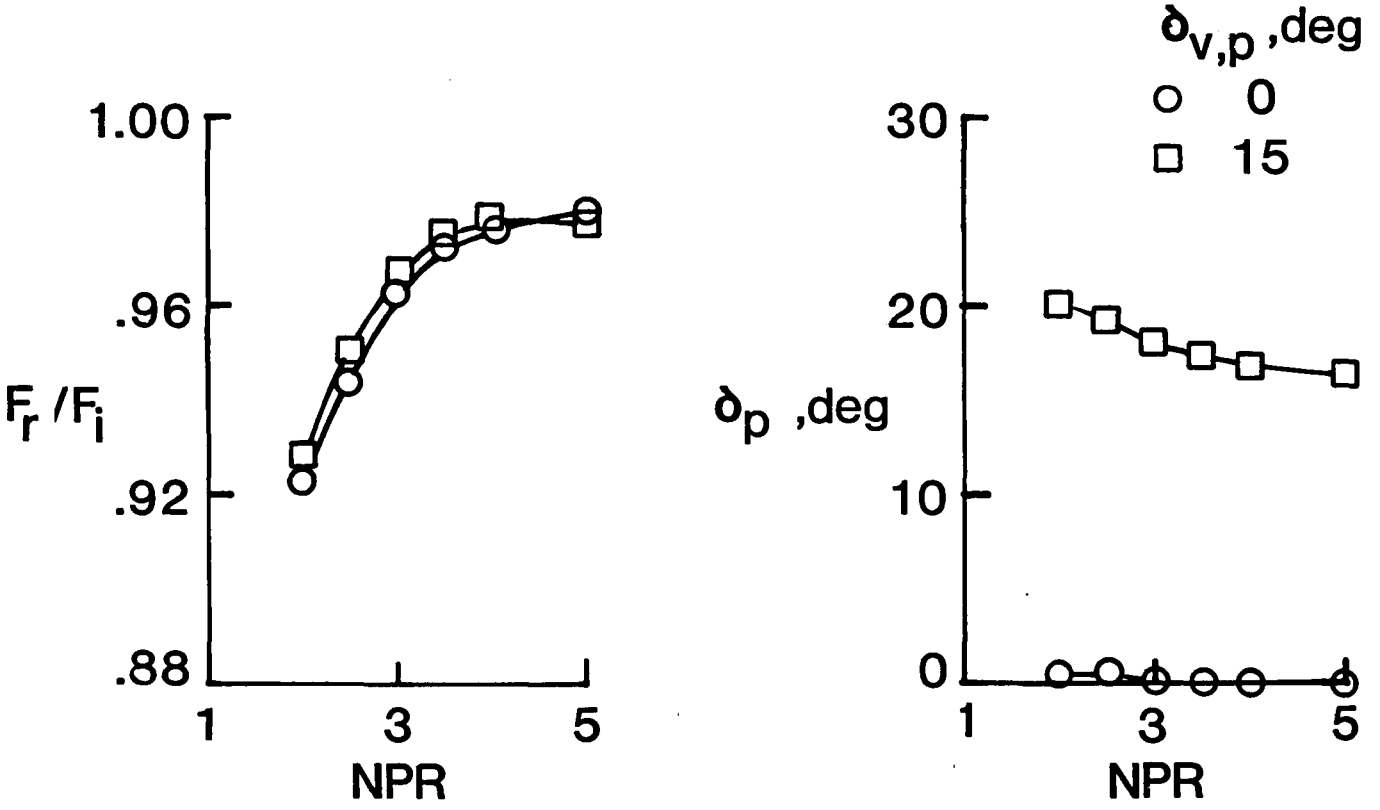

Figure 3.- Variation of static performance with nozzle pressure ratio configuration 1, A/B power, $\alpha = 0^{o}$.

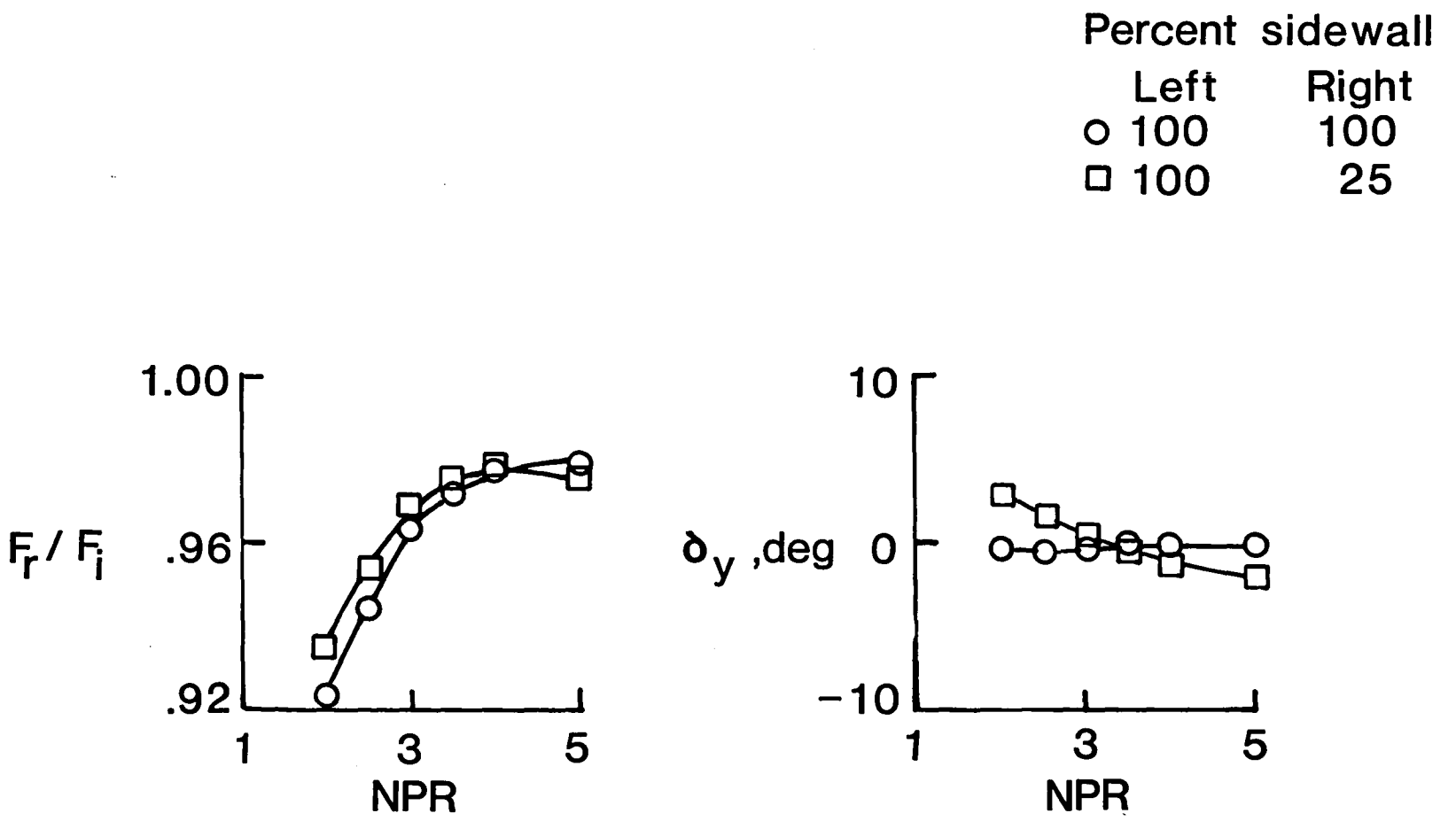

Figure 4.- Variation of static performance with yaw vectoring, configuration 1, A/B power, $\alpha = 0^{o}$.

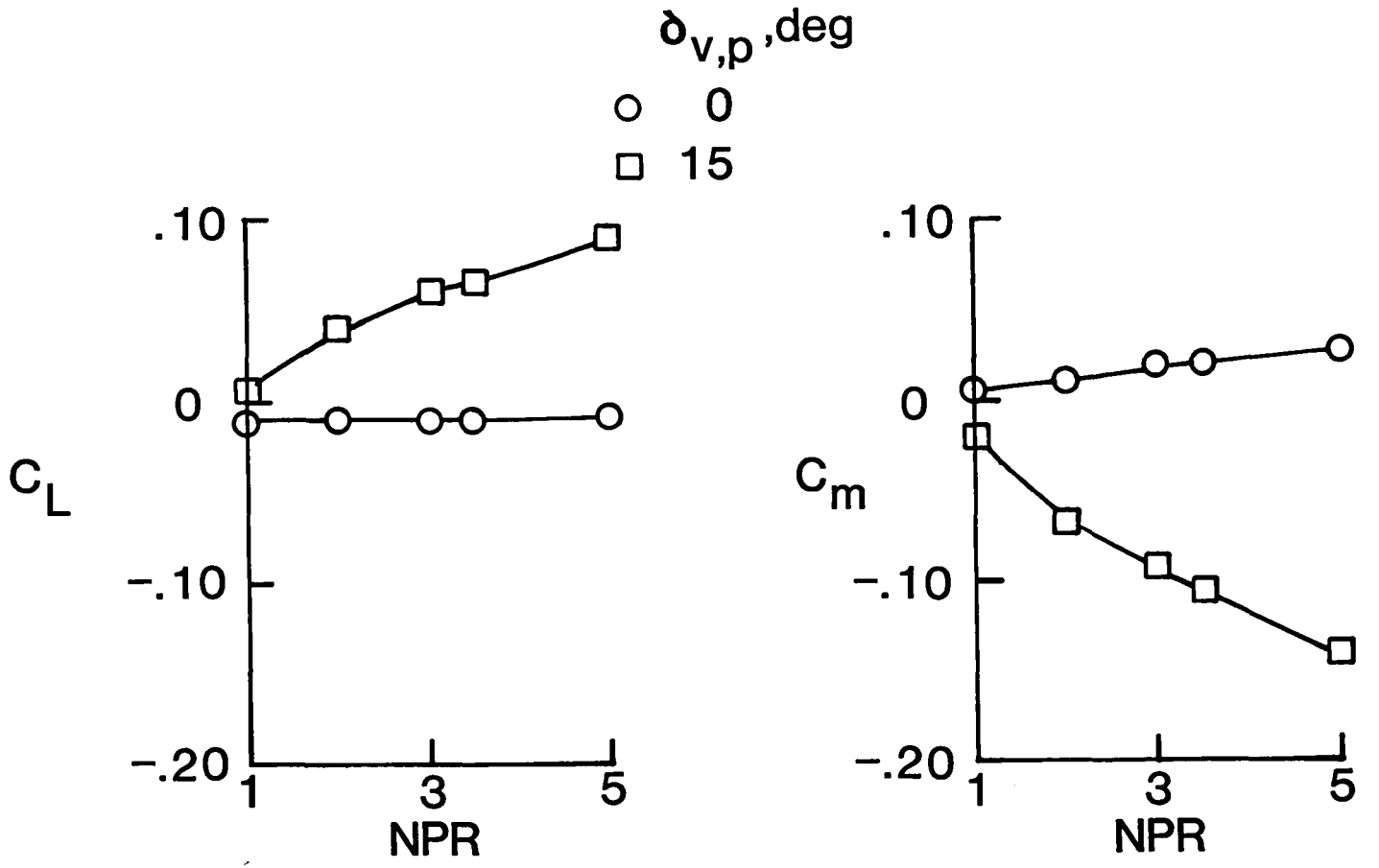

Figure 5.- Variation of longitudinal characteristics with nozzle pressure ratio, configuration 1, A/B power, M = 0.60, $\alpha = 0^{o}$.

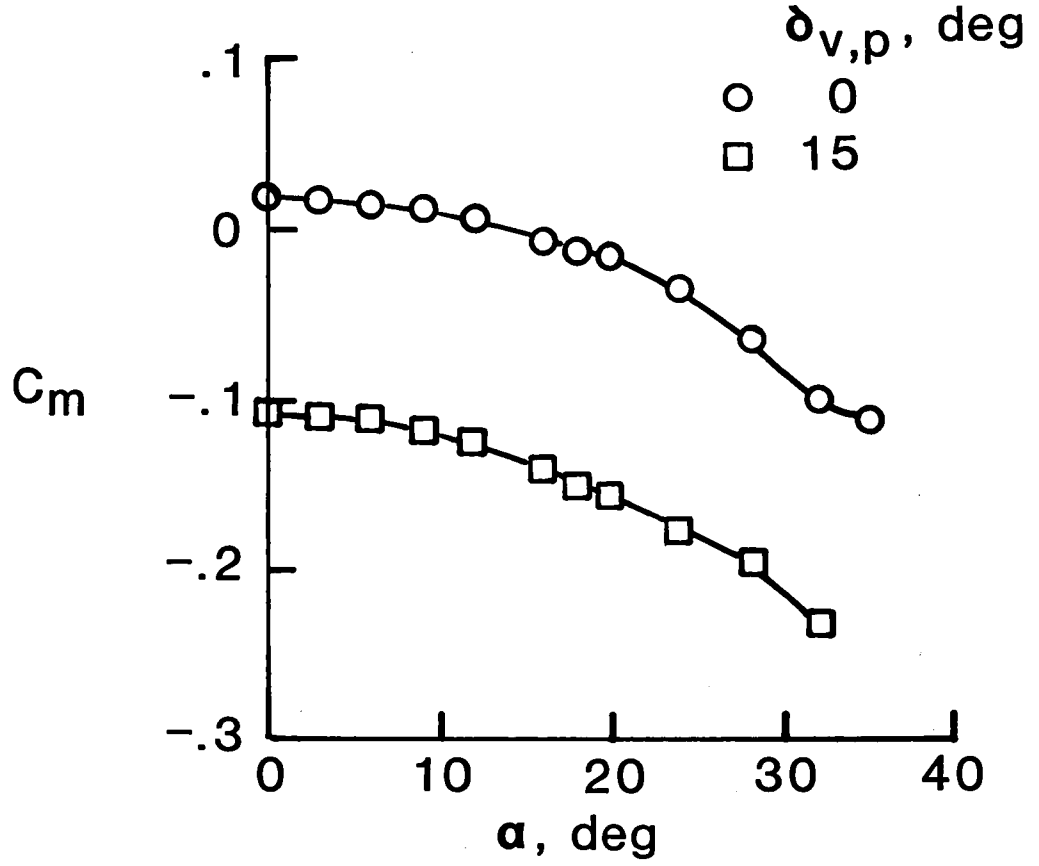

Figure 6.- Variation of pitching moment with angle of attack, configuration 1, A/B power, M = 0.60, NPR = 3.5.

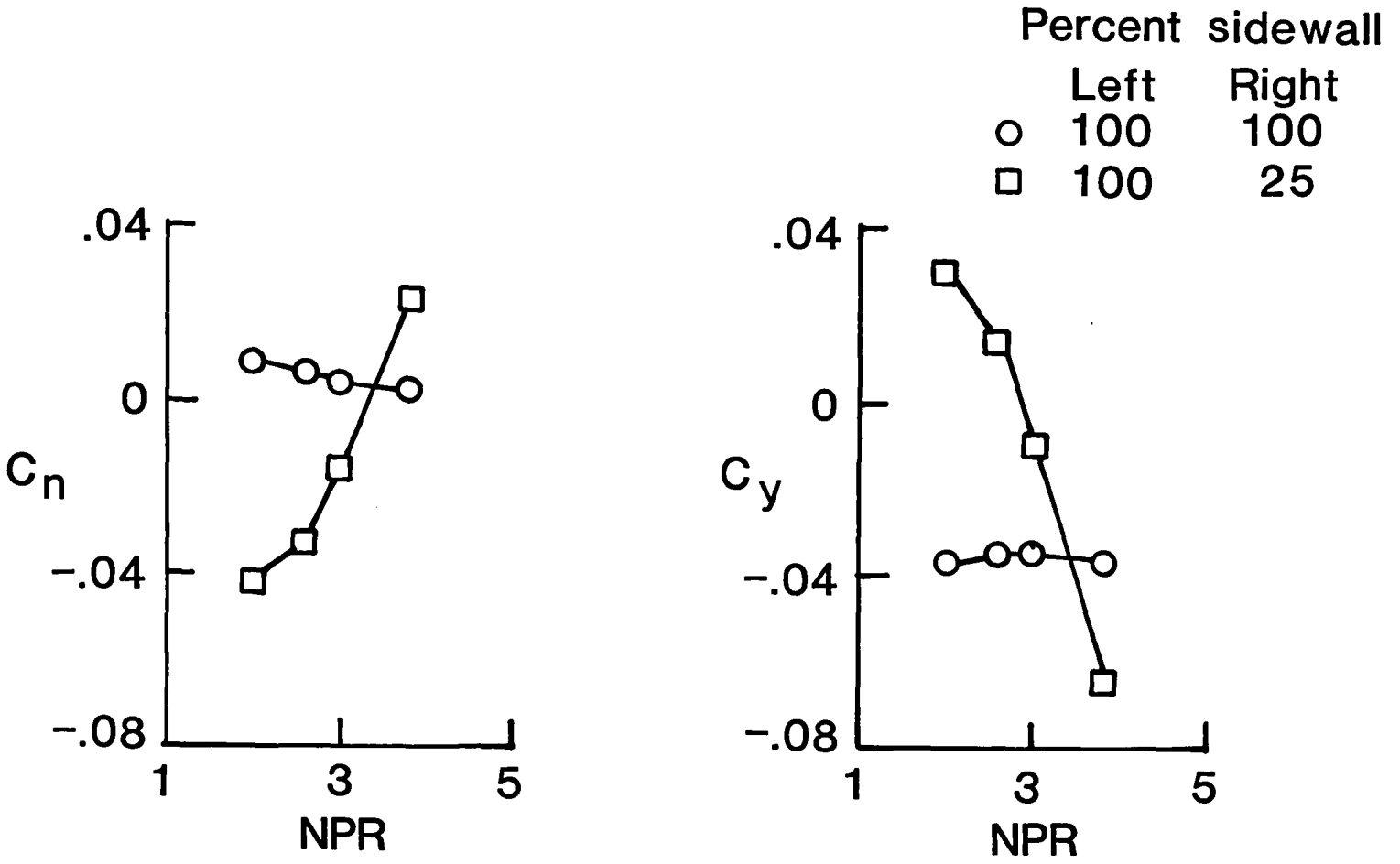

Figure 7.- Variation of lateral characteristics with nozzle pressure ratio, configuration 1, A/B power, M = 0.15, $\alpha = 0^{o}$.

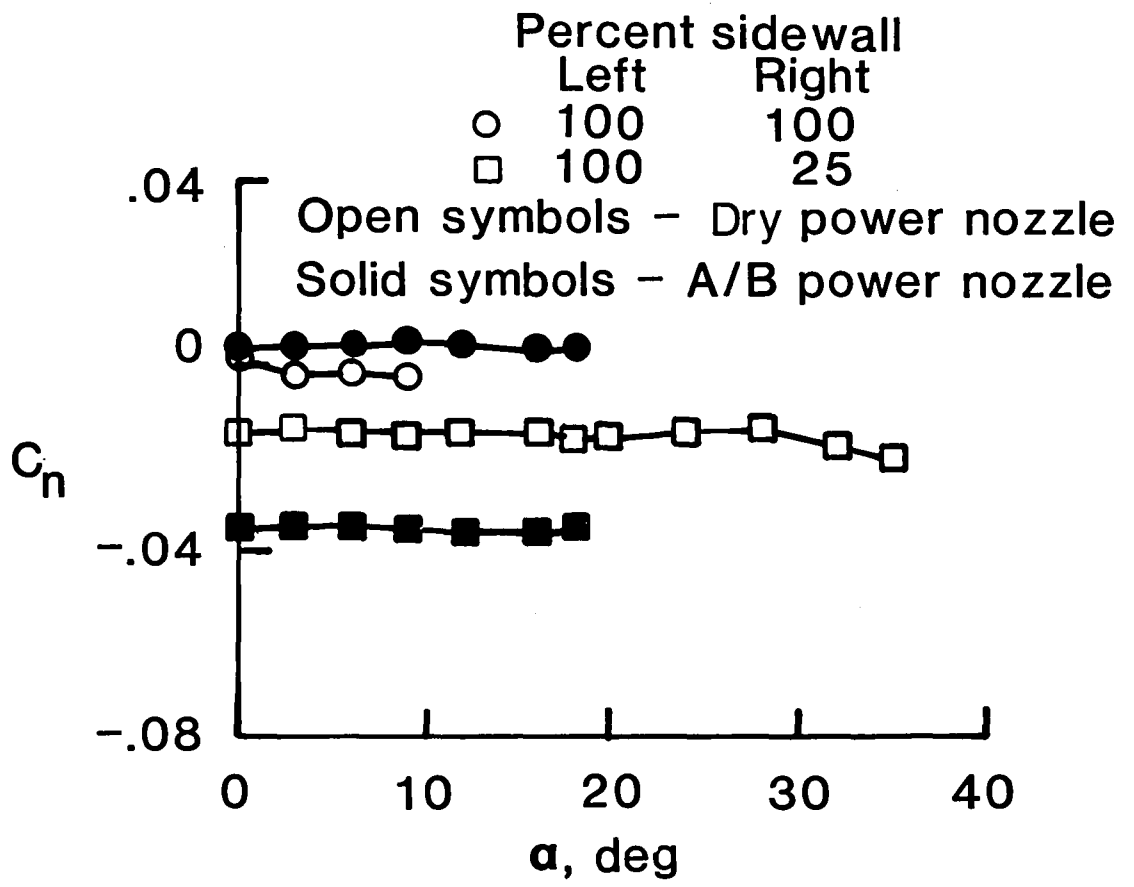

Figure 8.- Variation of yawing moment with angle of attack, configuration 1, M = 0.15, NPR = 2.6.

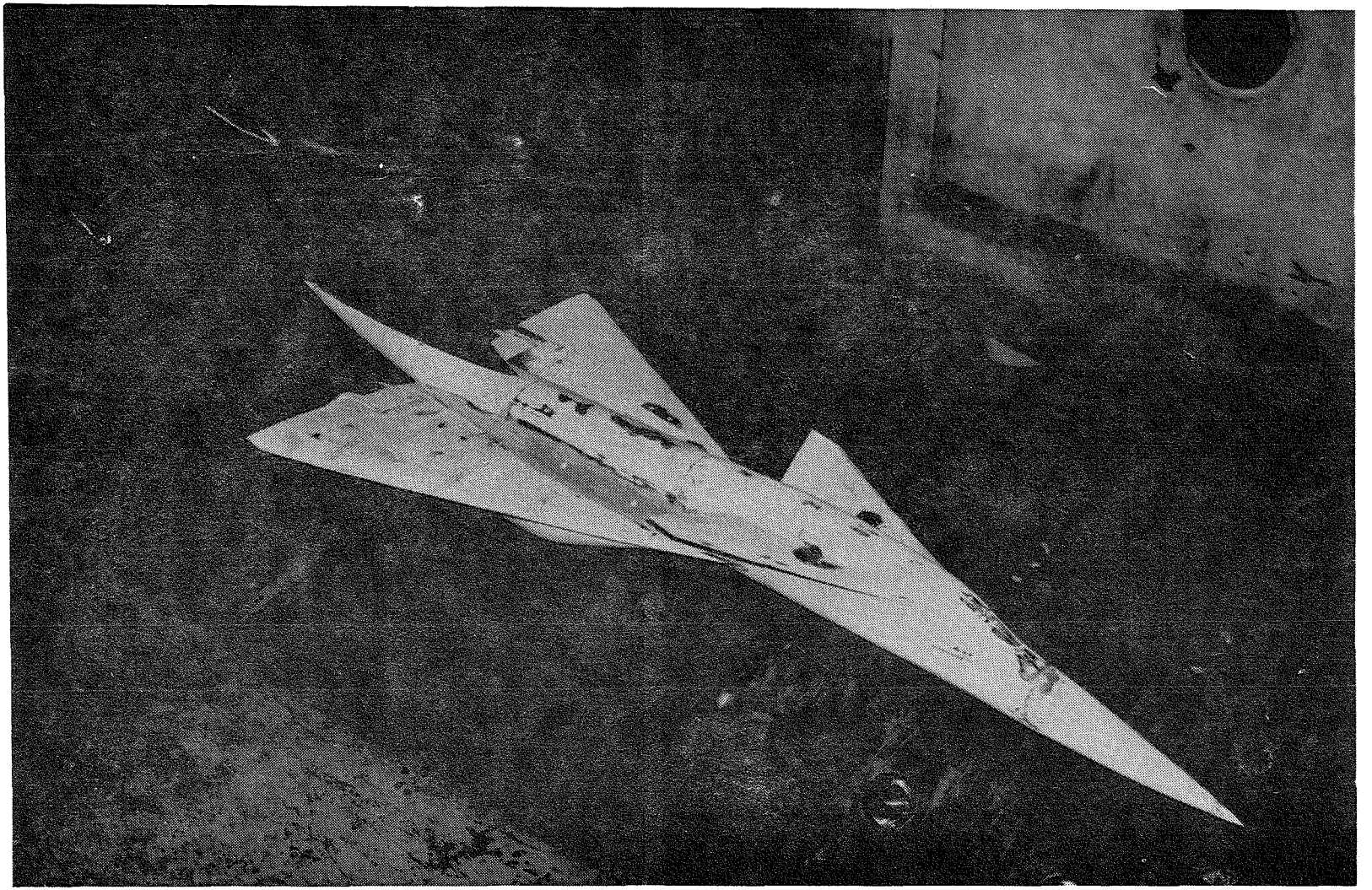

Figure 9.- Configuration 2, supercruise model.

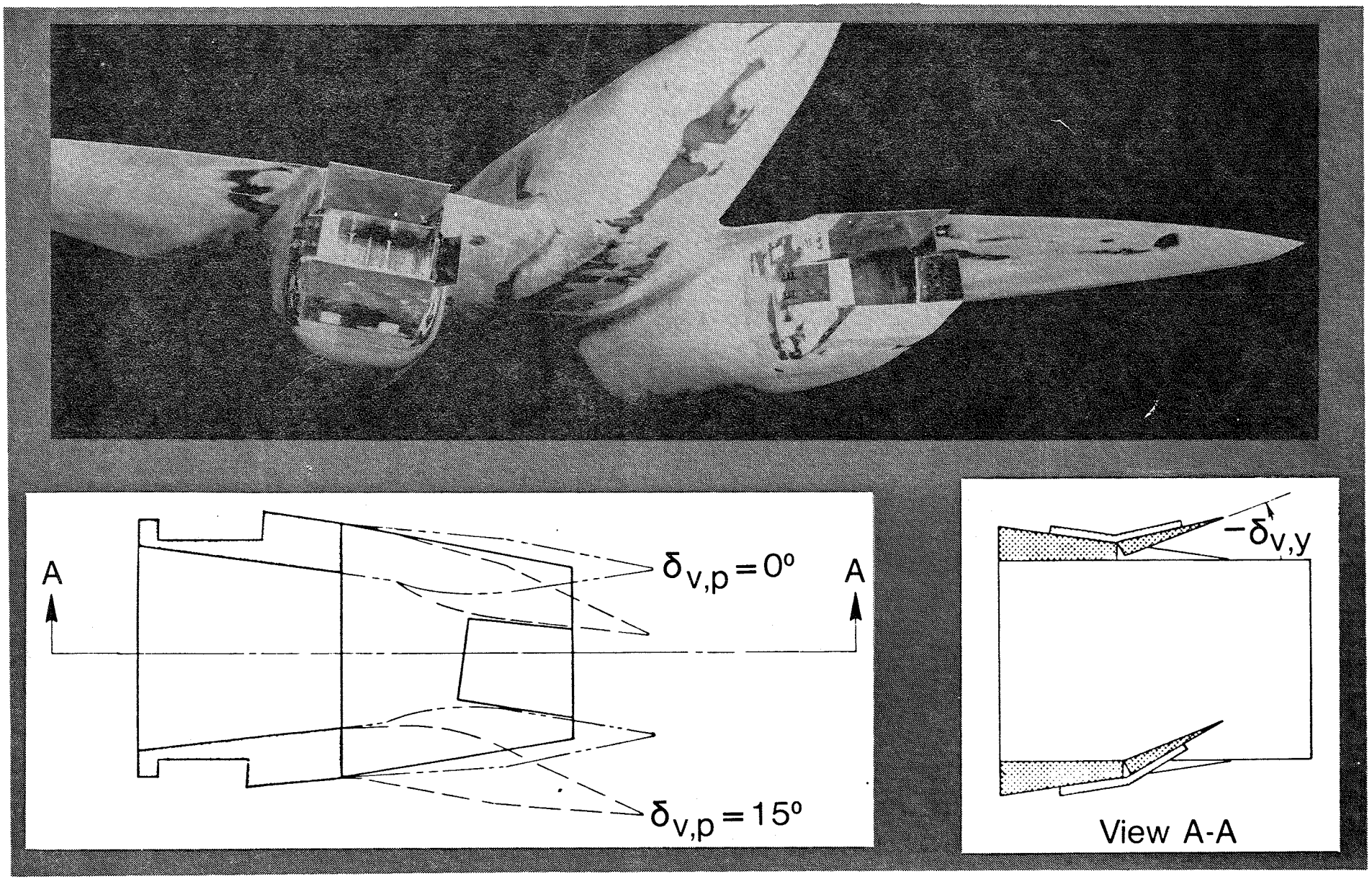

Figure 10.- Configuration 2, 2-D C-D nozzle geometry, A/B power.

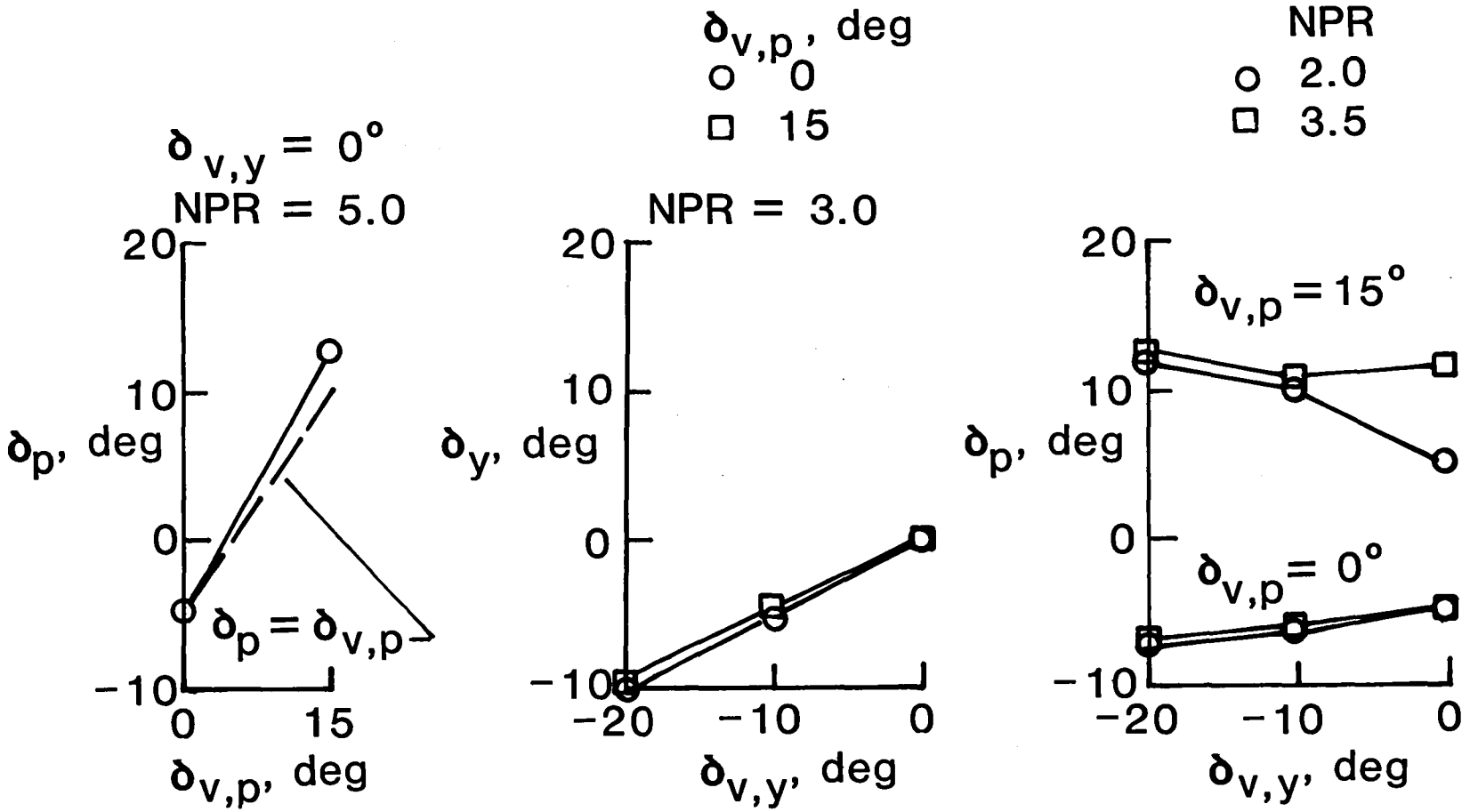

Figure 11.- Resultant thrust vector angles, configuration 2, A/B power, M = 0.

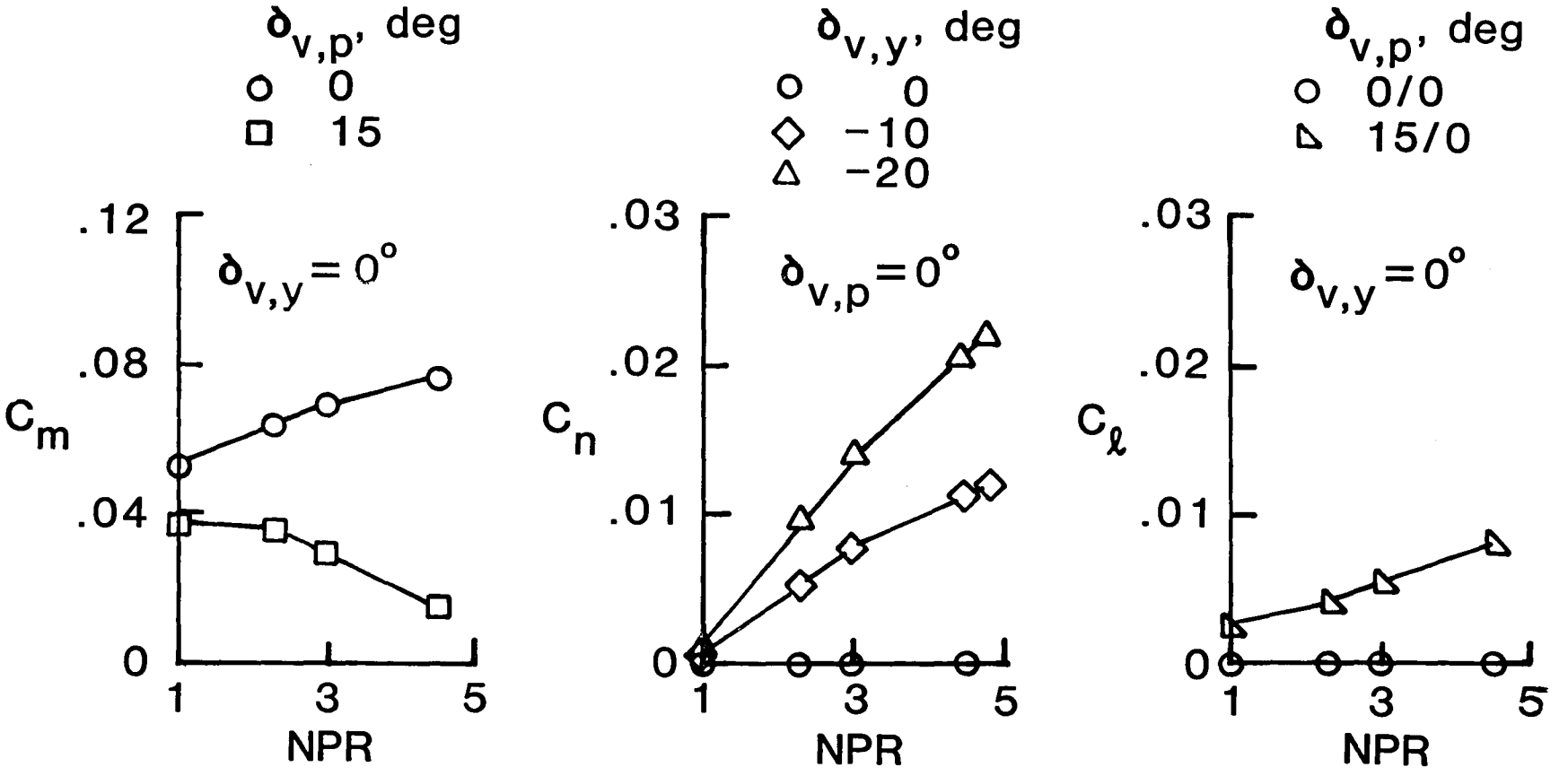

Figure 12.- Variation of control moments with nozzle pressure ratio, configuration 2, A/B power, M = 0.60, $\alpha = 4^{o}$.

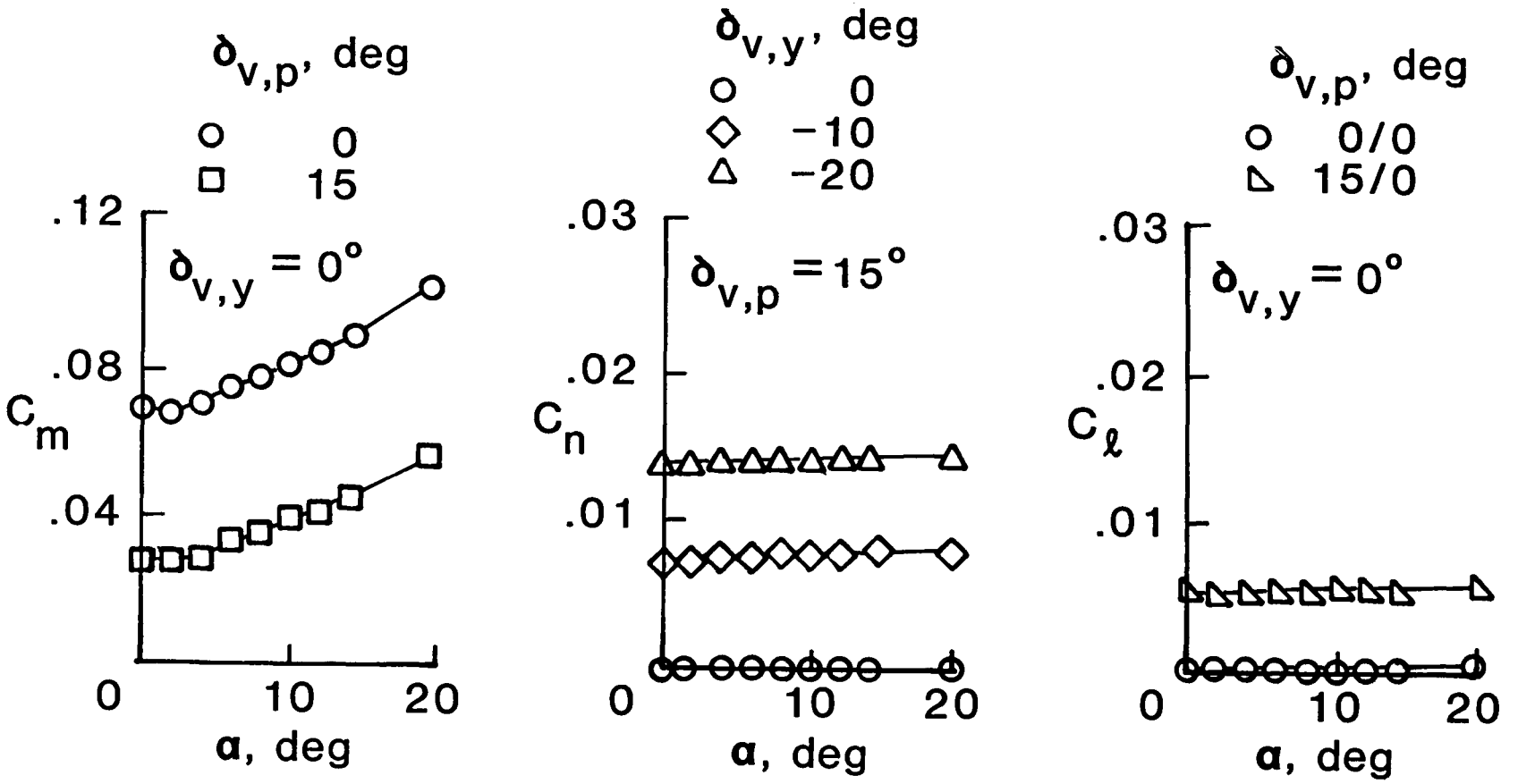

Figure 13.- Variation of control moments with angle of attack, configuration 2, A/B power, M = 0.60, NPR = 3.0.

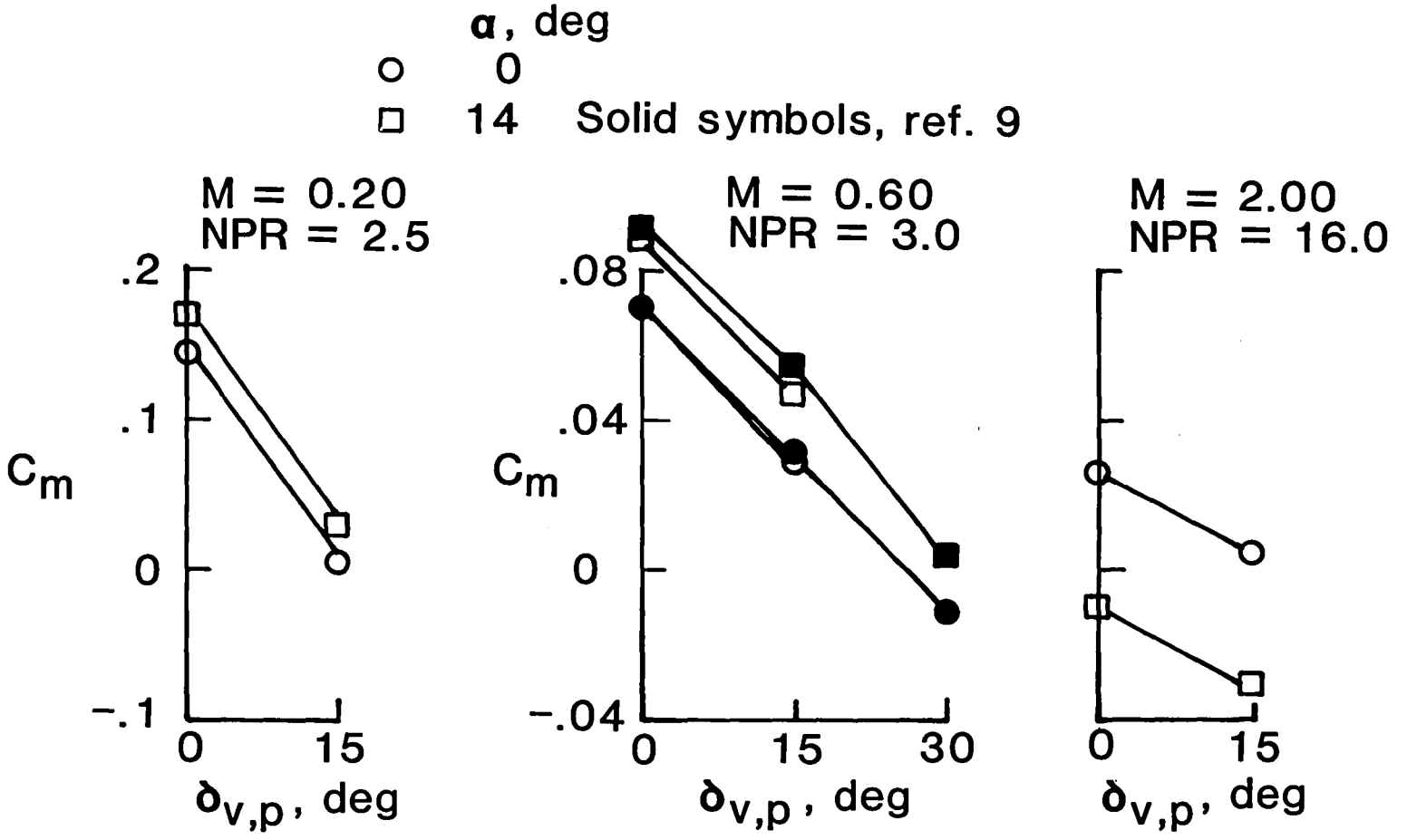

Figure 14.- Variation of pitching moment with pitch vector angle, configuration 2, A/B power, $\delta_{v,y} = 0^{o}$.

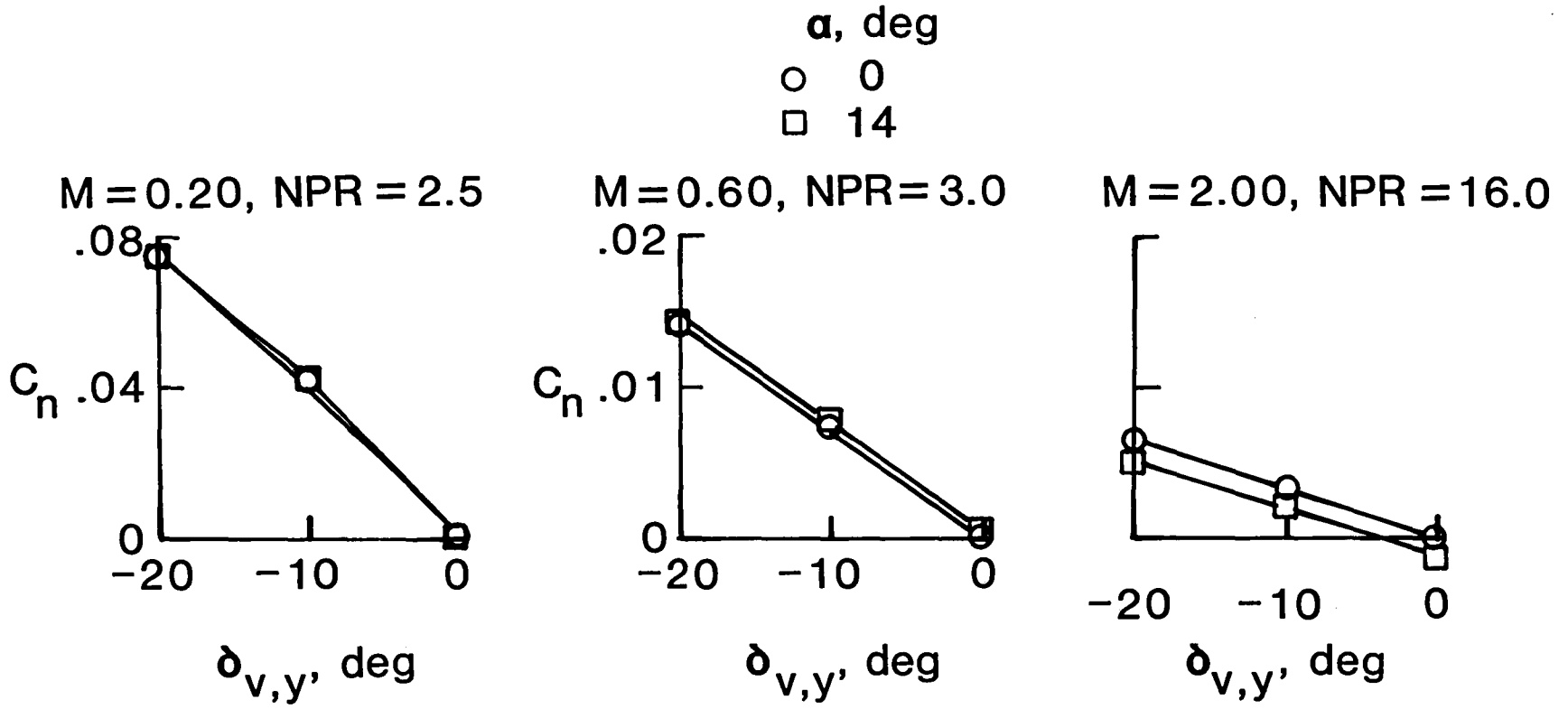

Figure 15.- Variation of yawing moment with yaw vector angle, configuration 2, A/B power, $\delta_{v,p} = 0^{o}$.

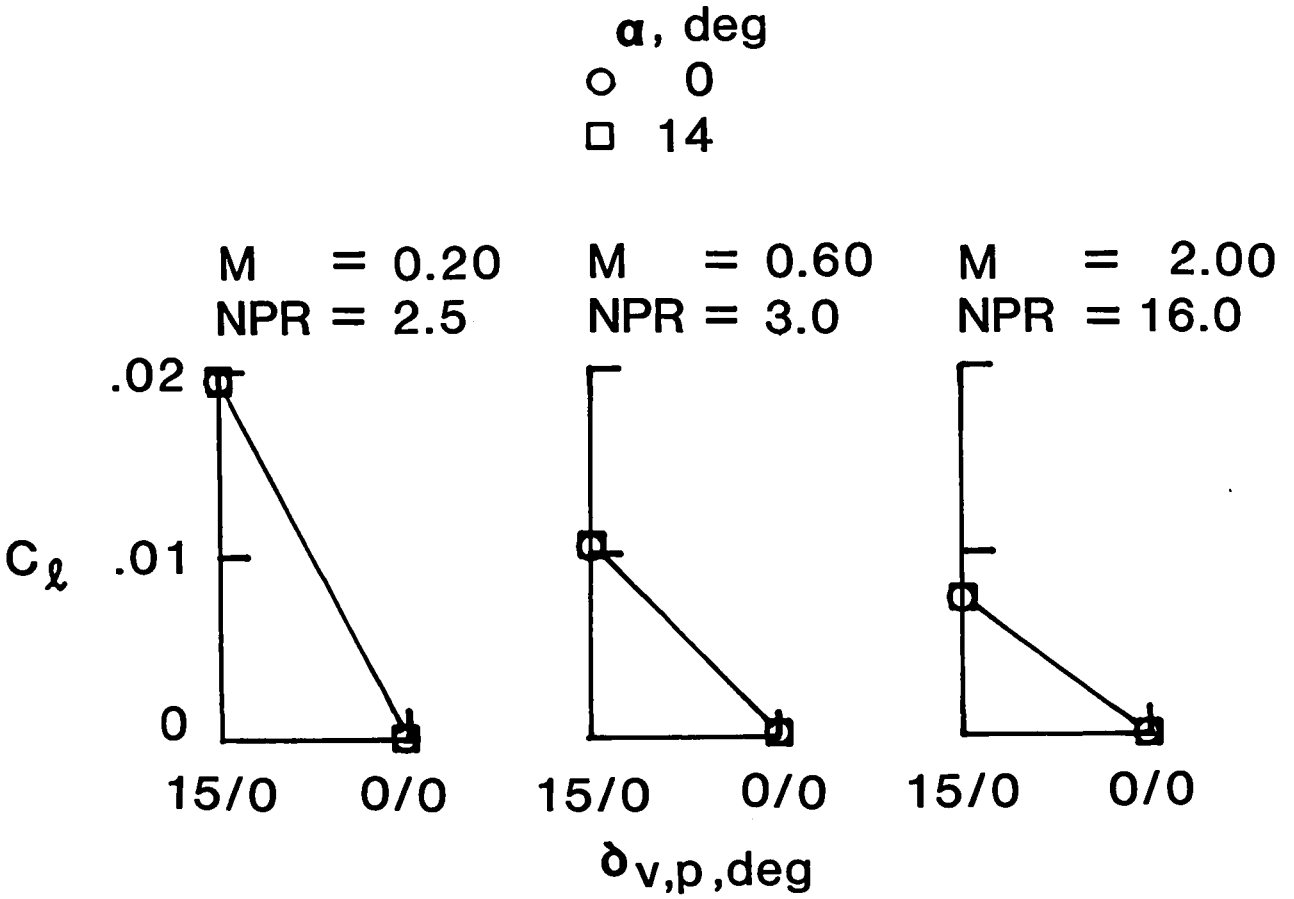

Figure 16.- Variation of rolling moment with differential pitch vector angle, configuration 2, A/B power, $\delta_{v,y} = 0^o$.

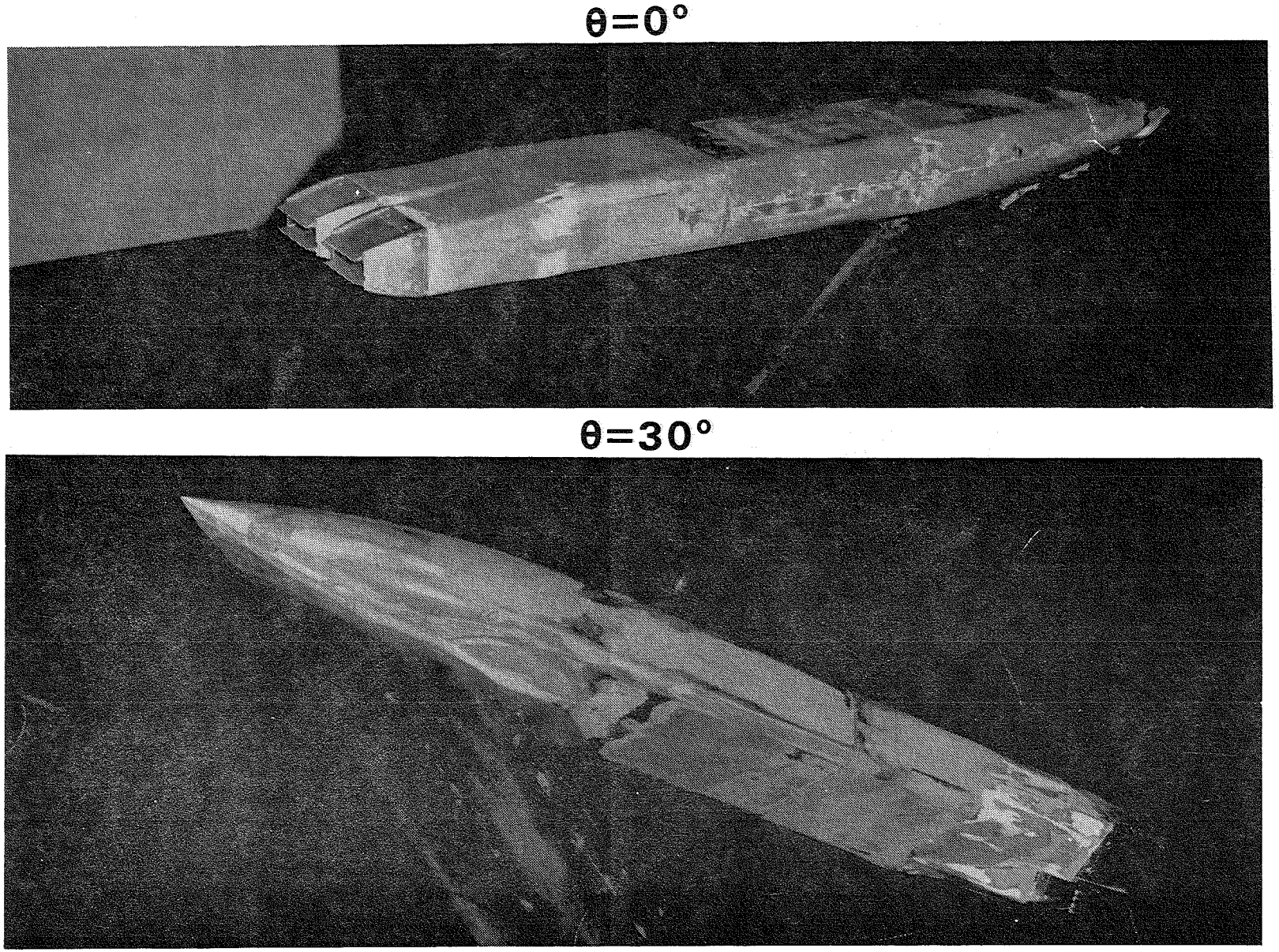

Figure 17.- Configuration 3, powered control enhancement model.

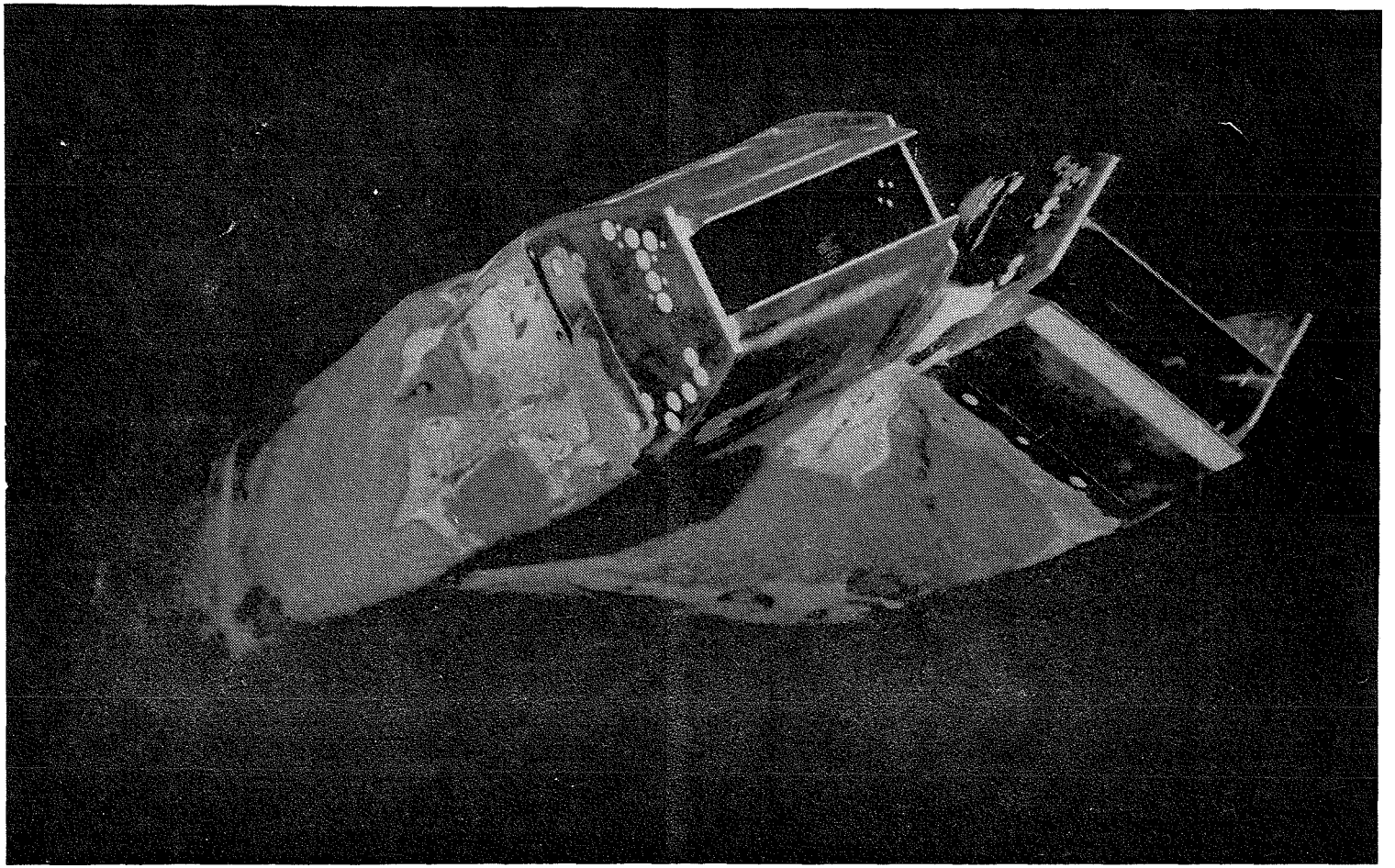

Figure 18.- Configuration 3, nozzles canted 30^{o}, $\delta_{v,p} = 0^{o}/20^{o}$.

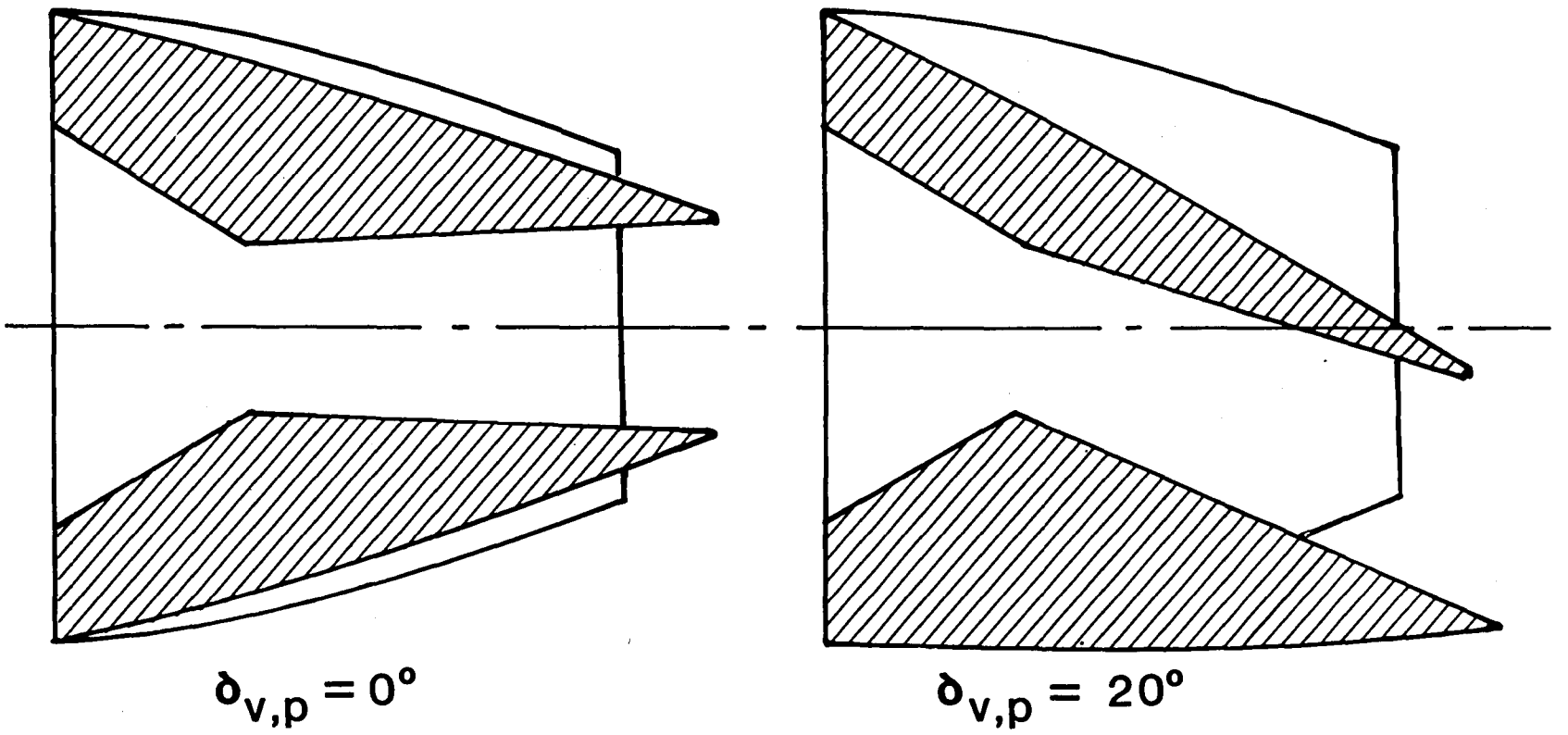

Figure 19.- Configuration 3, 2-D C-D nozzle geometry, dry power.

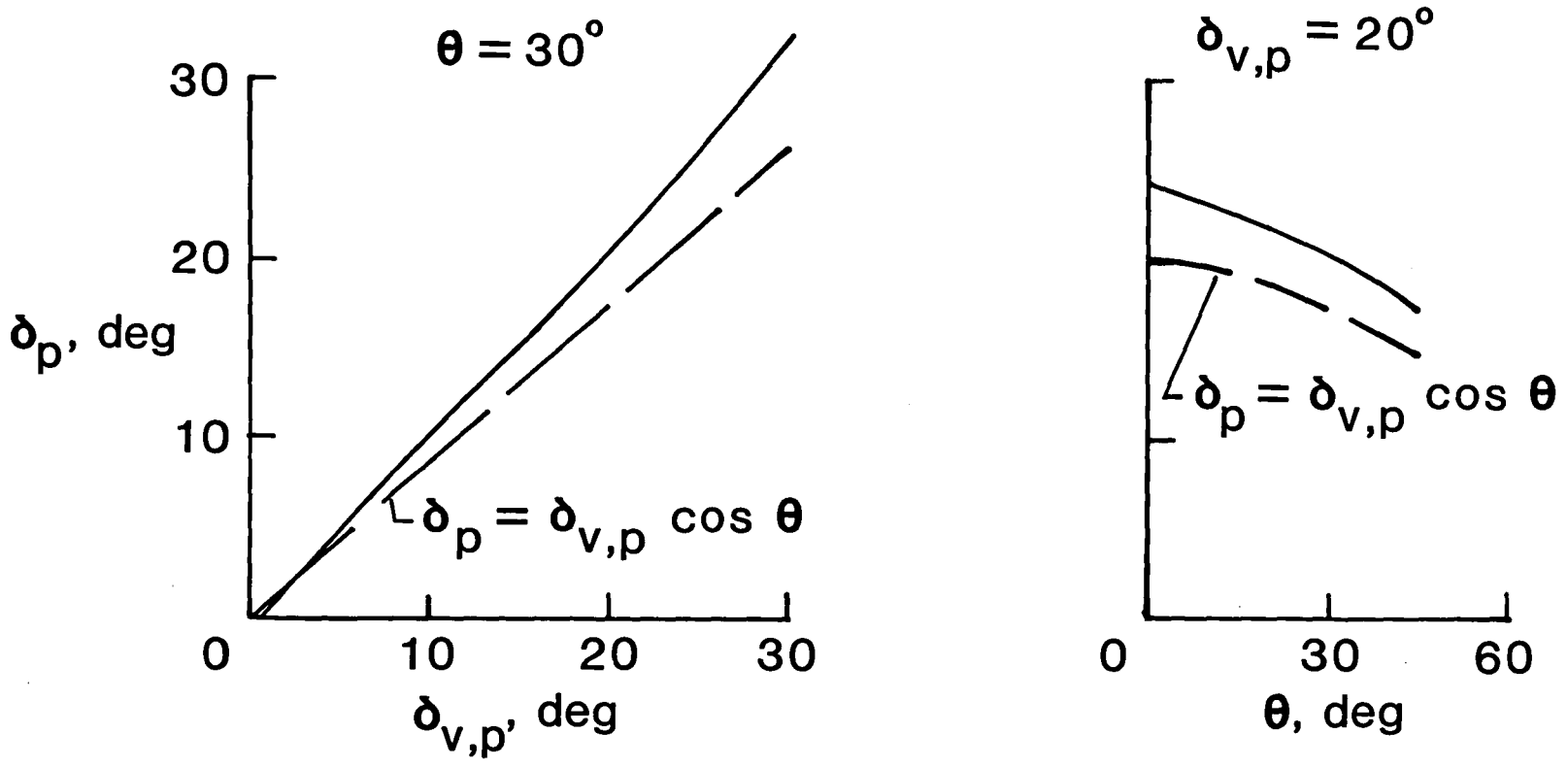

Figure 20.- Resultant pitch vector angles, configuration 3, dry power, M = 0, NPR = 3.2.

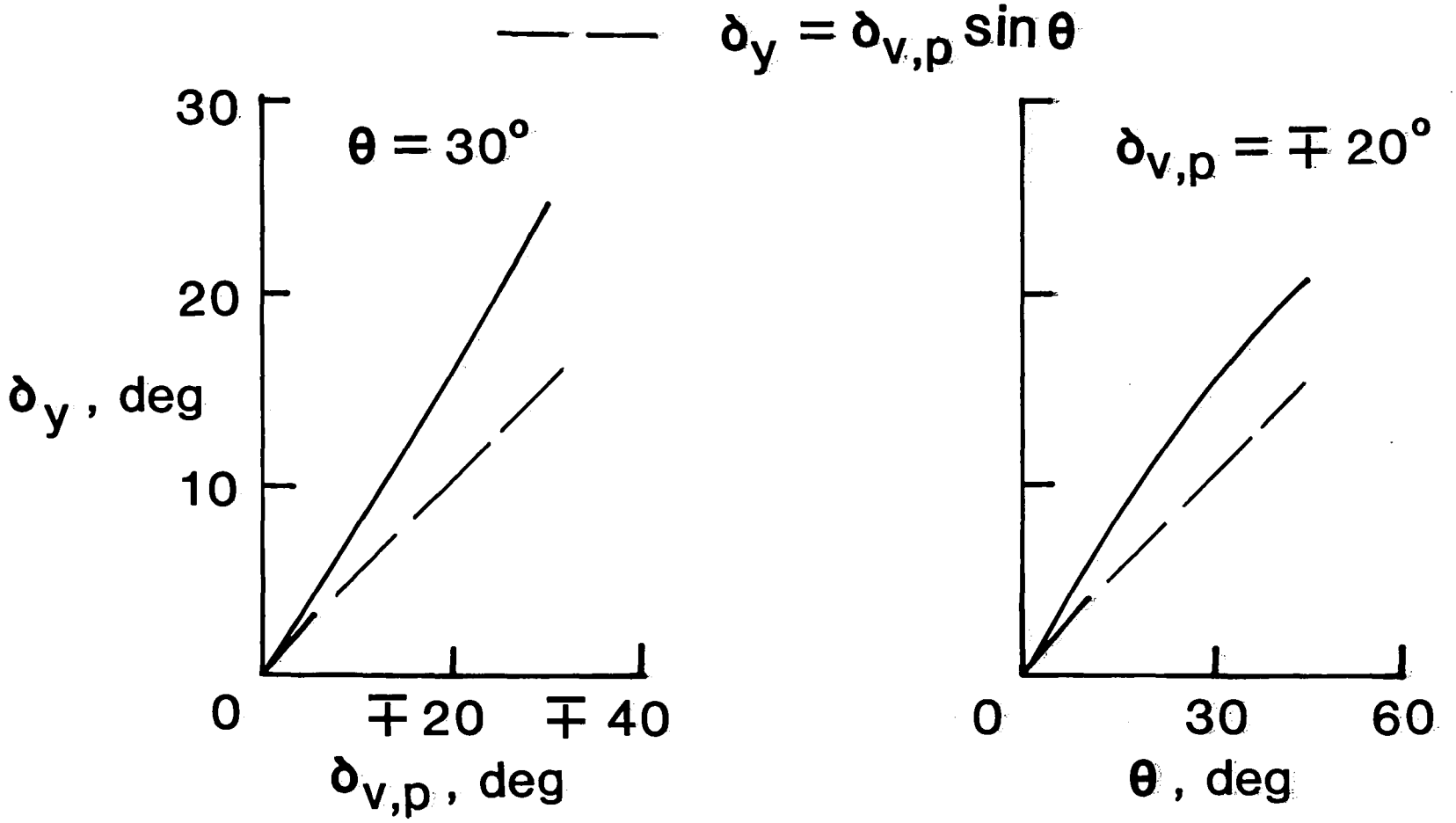

Figure 21.- Resultant yaw thrust vector angles, configuration 3, dry power, M = 0, NPR = 3.2.

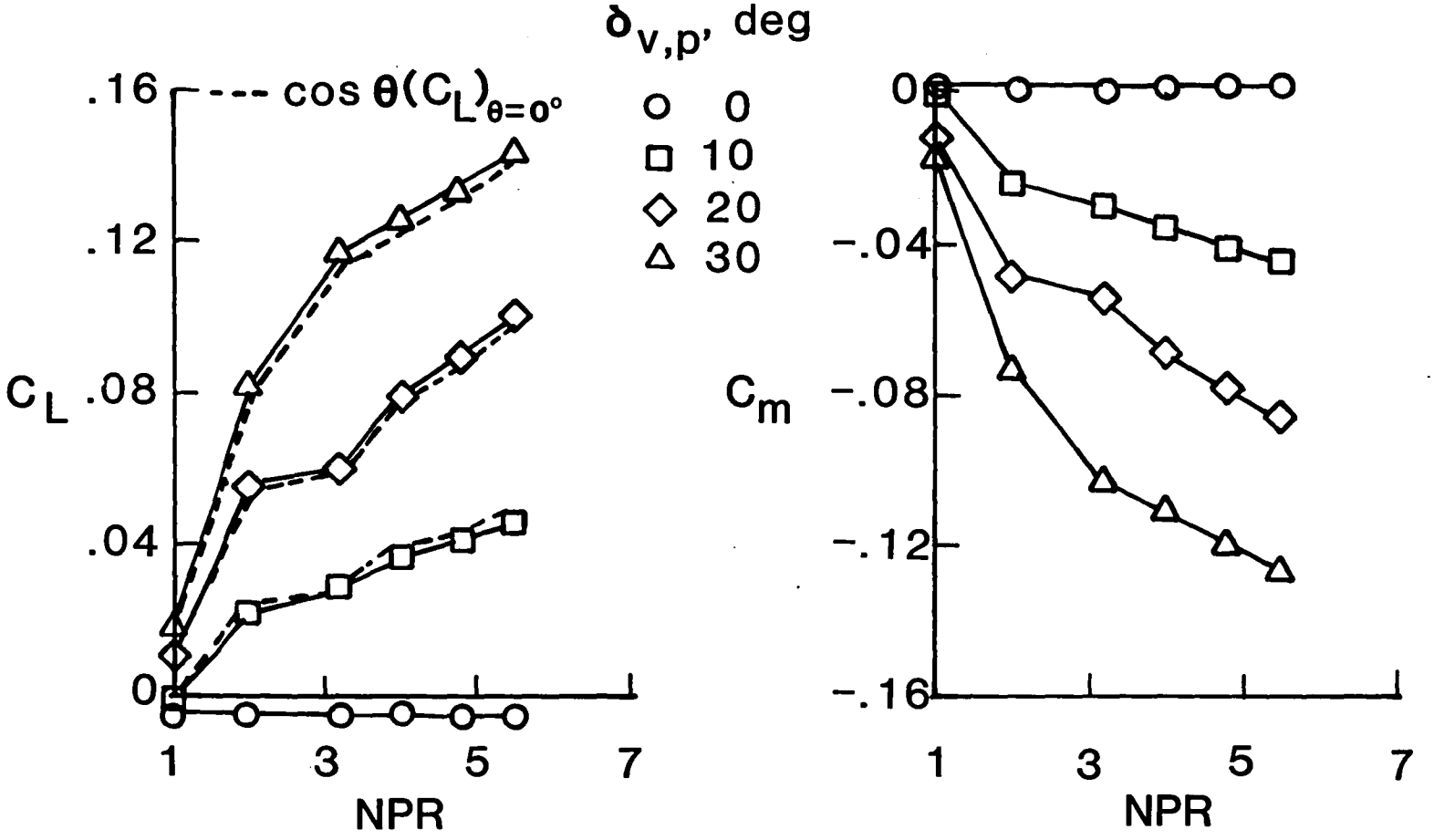

Figure 22.- Variation of lift and pitching moment with nozzle pressure ratio, configuration 3, dry power, $\theta = 30^\circ$, M = 0.60, $\alpha = 0^\circ$.

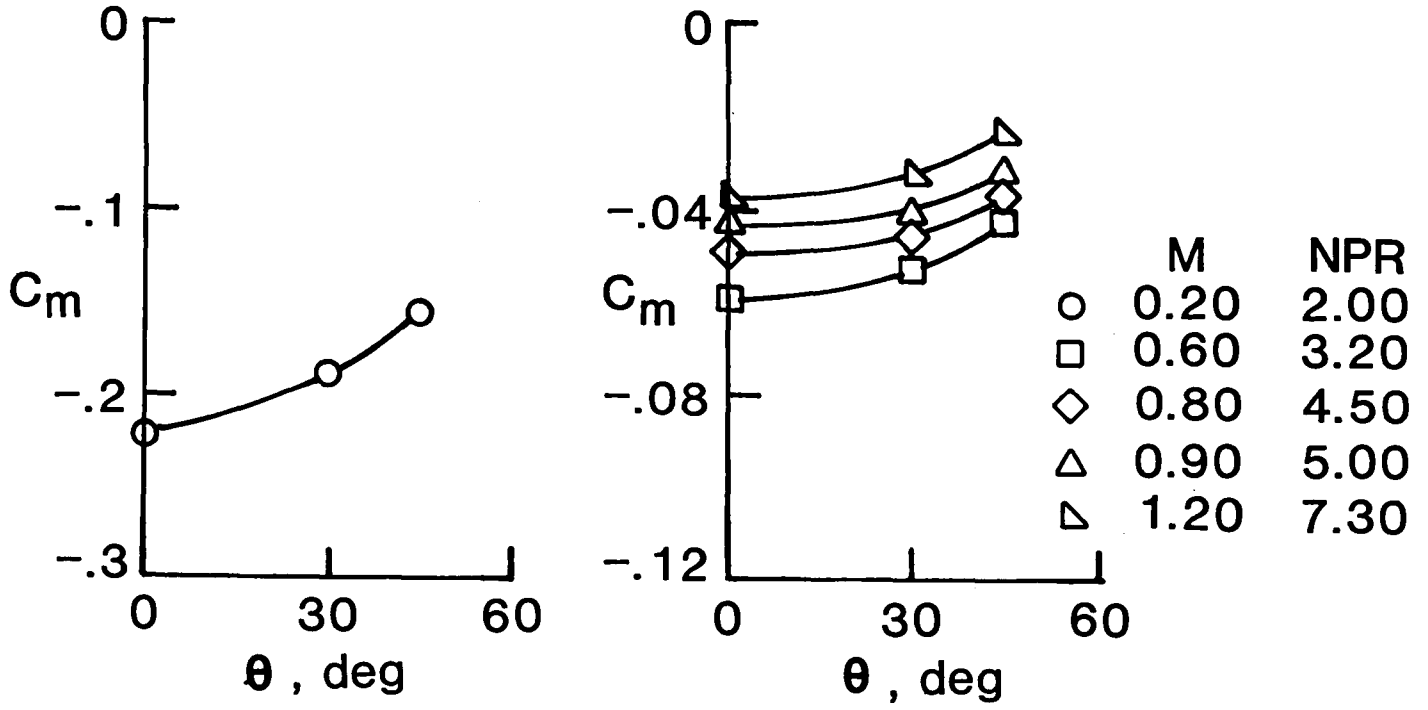

Figure 23.- Variation of pitching moment with nozzle cant angle configuration 3, dry power, $\delta_{v,p} = 20^{o}$, $\alpha = 0^{o}$.

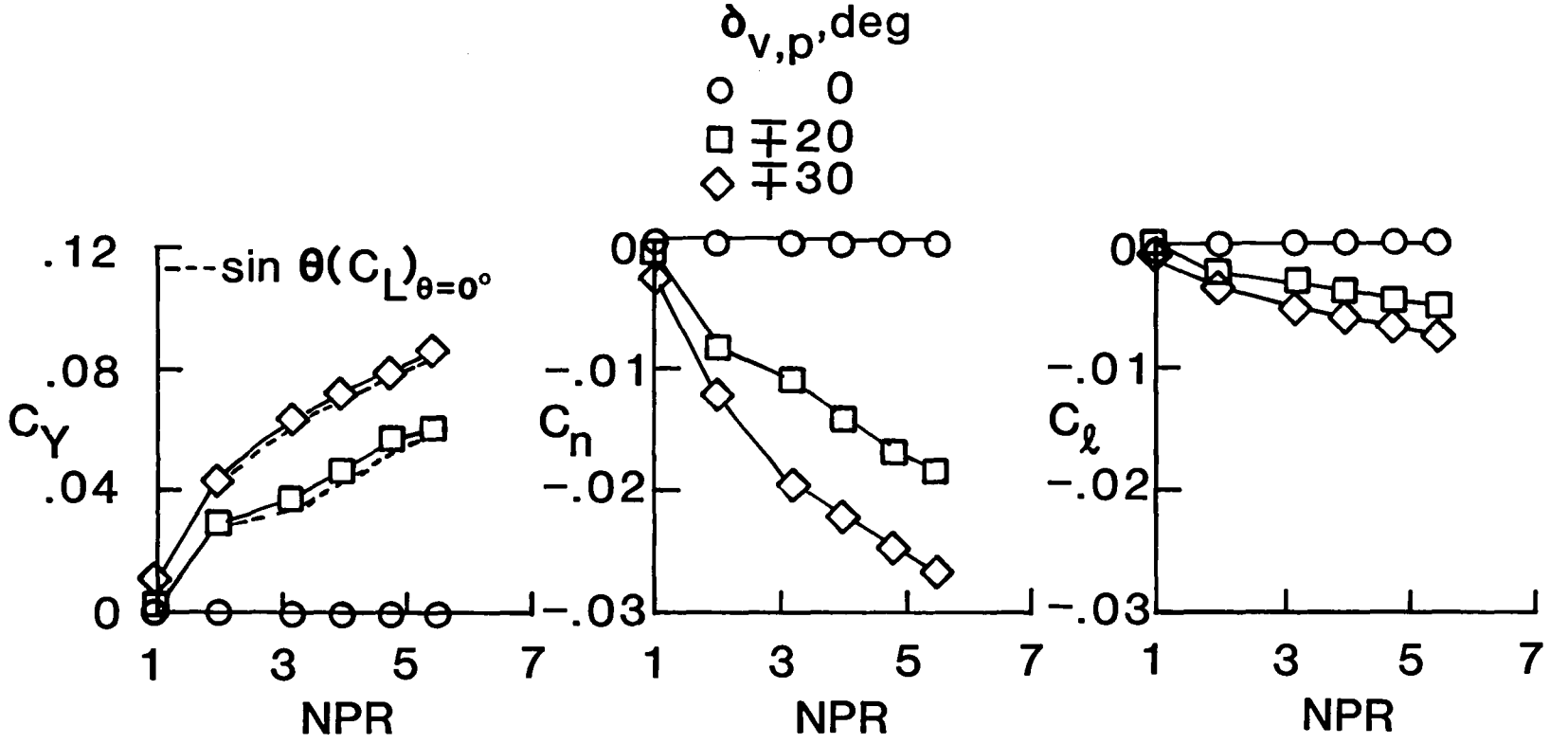

Figure 24.- Variation of lateral characteristics with differential pitch vector angle, configuration 3, dry power, $\theta = 30^{o}$, M = 0.60, $\alpha = 0^{o}$.

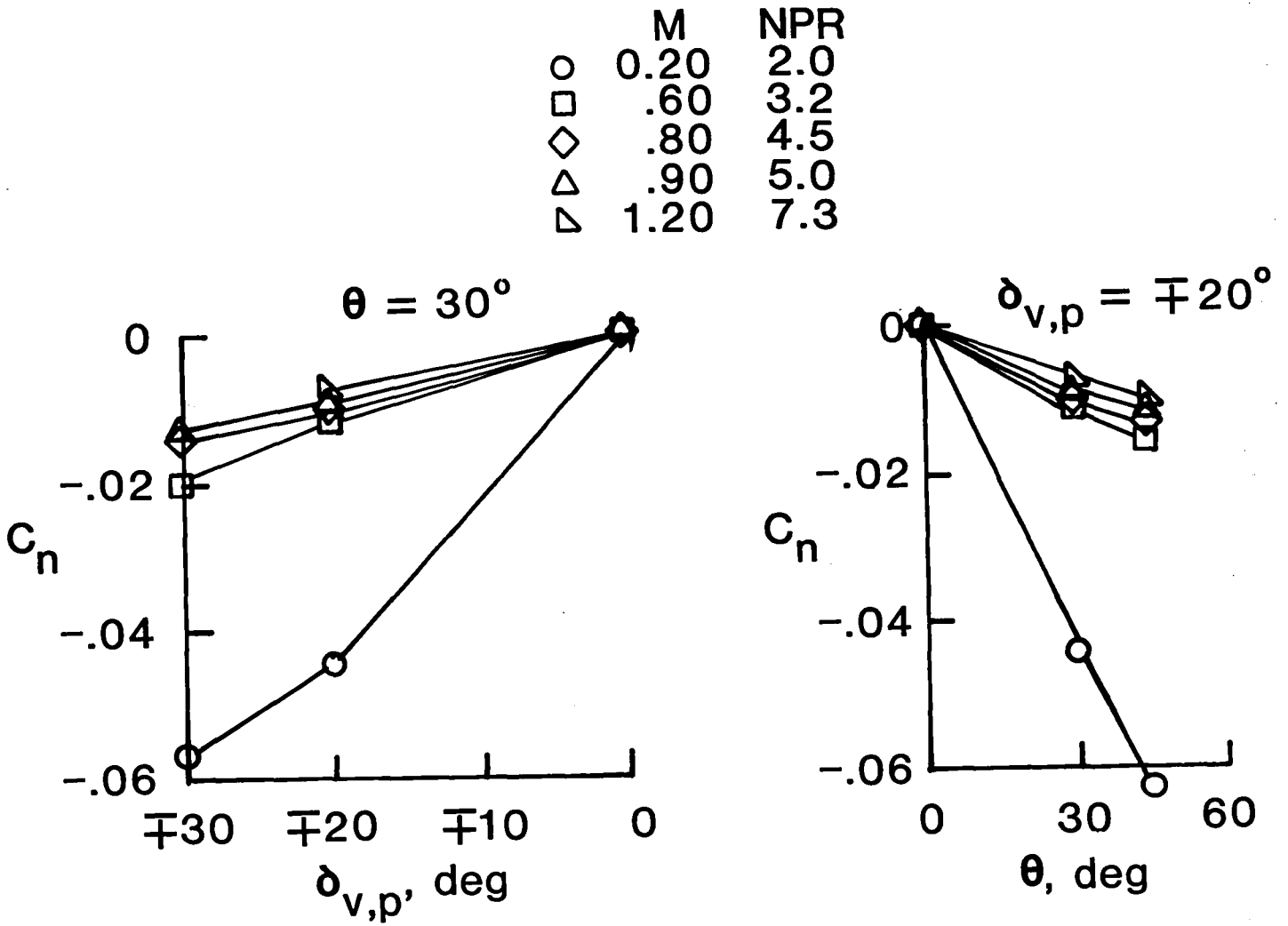

Figure 25.- Variation of yawing moment with $\delta_{v,p}$ and θ, configuration 3, dry power, $\alpha = 0^{o}$.

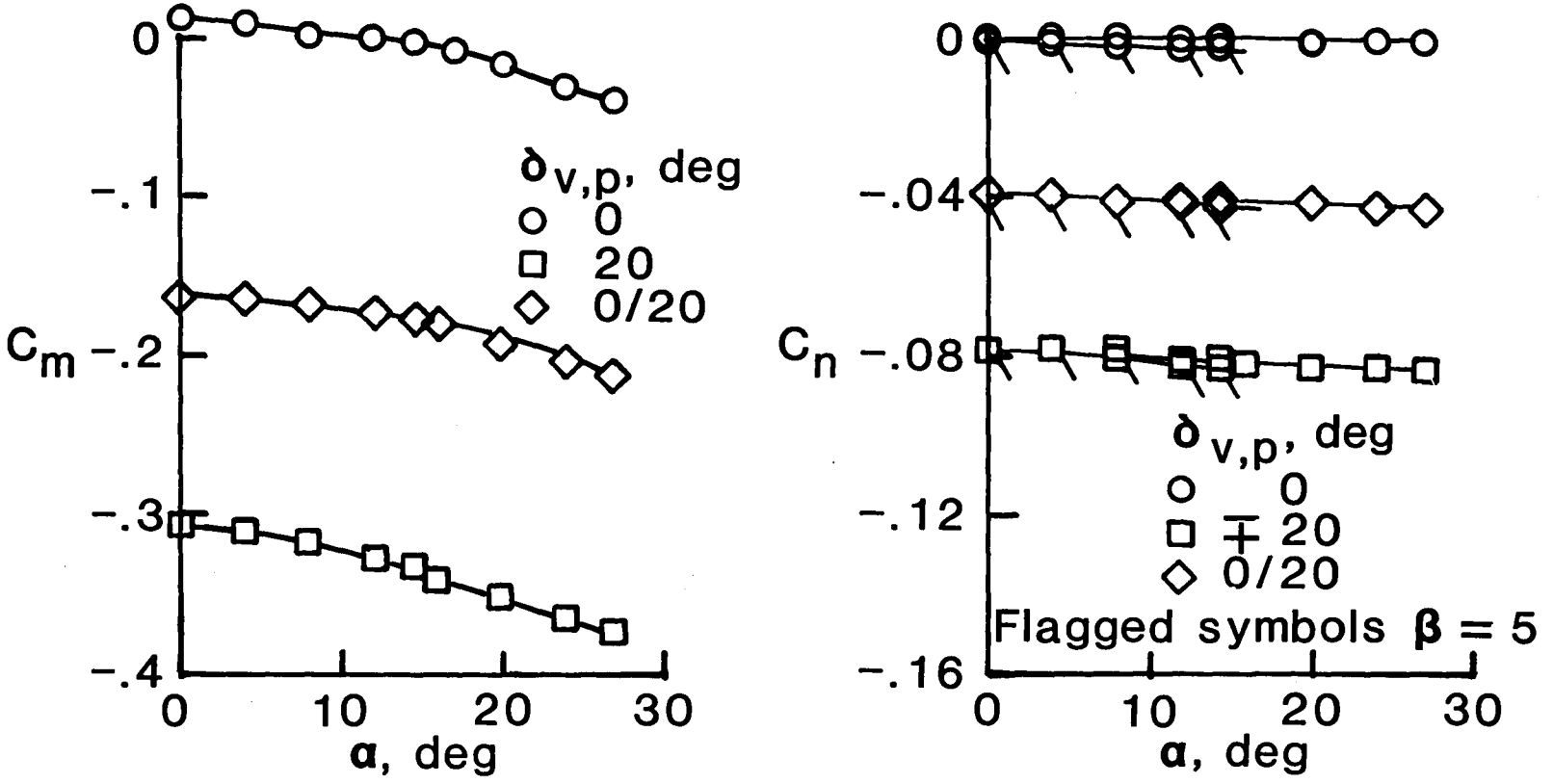

Figure 26.- Variation of pitch and yawing moment with angle of attack, configuration 3, dry power, $\theta = 30^{o}$, M = 0.20, $\alpha = 3.2$.

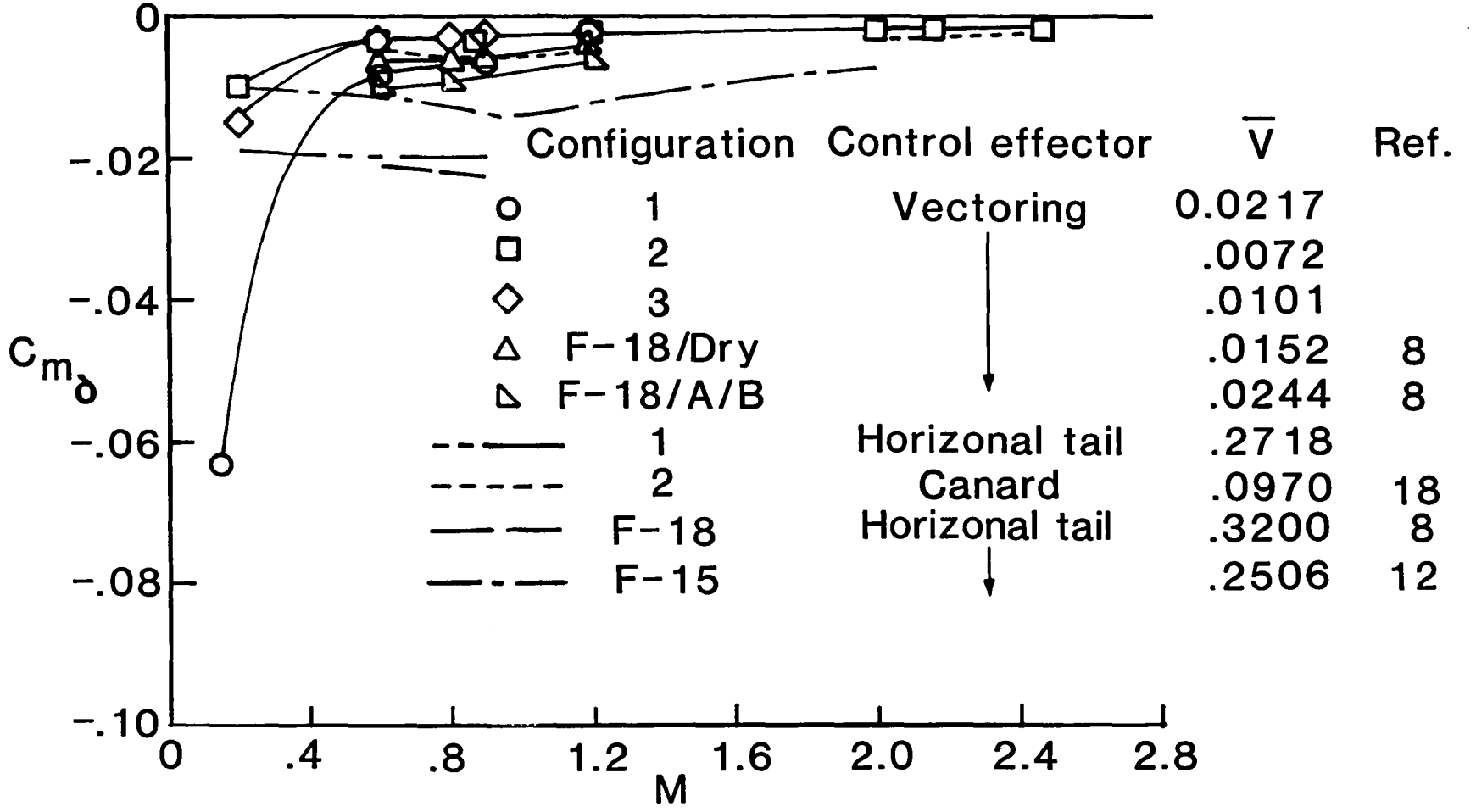

Figure 27.- Variation of longitudinal control power with Mach number, at scheduled NPR, $\alpha = 0^0$.

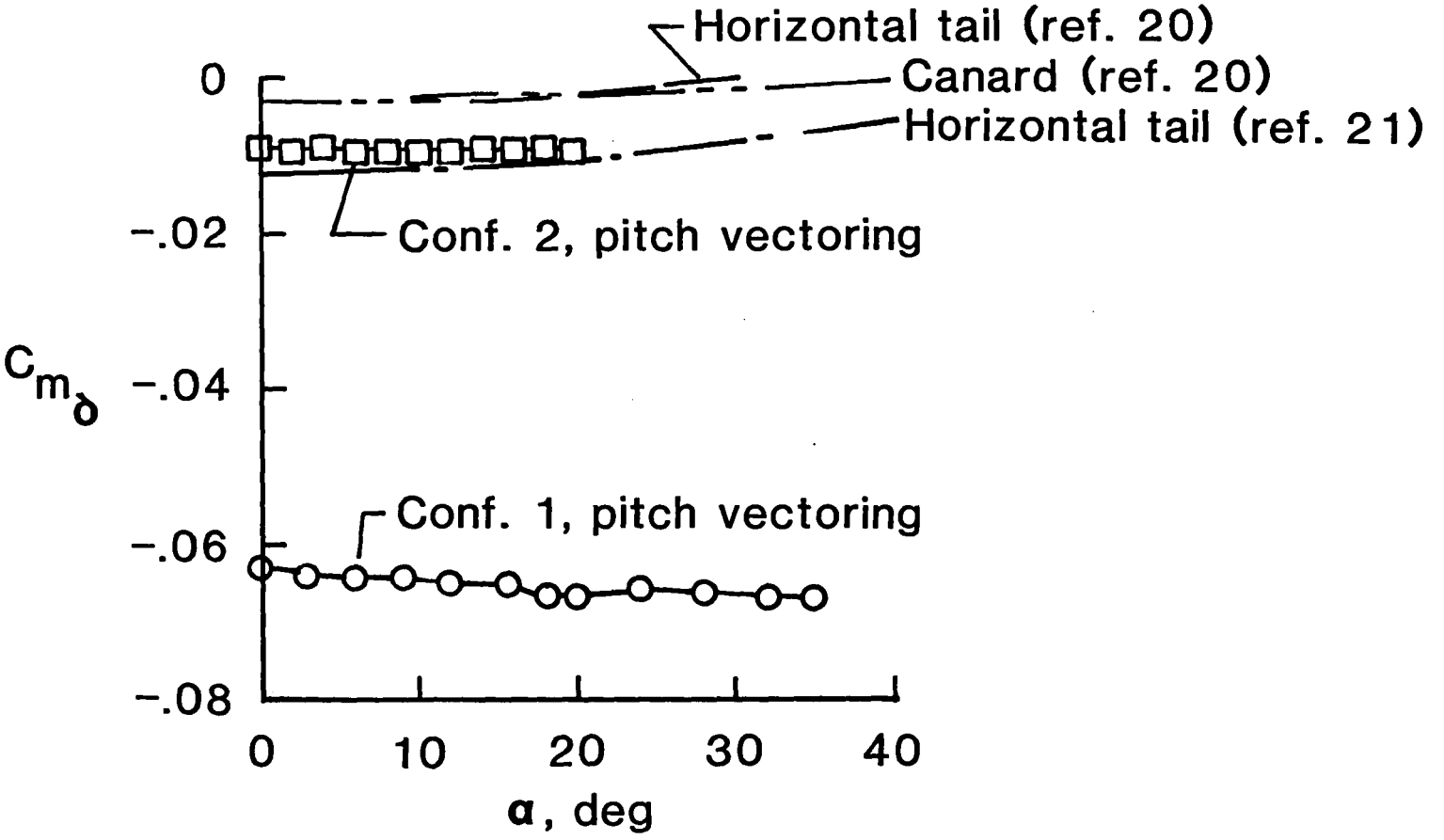

Figure 28.- Variation of longitudinal control power with angle of attack, at scheduled NPR, low speed.

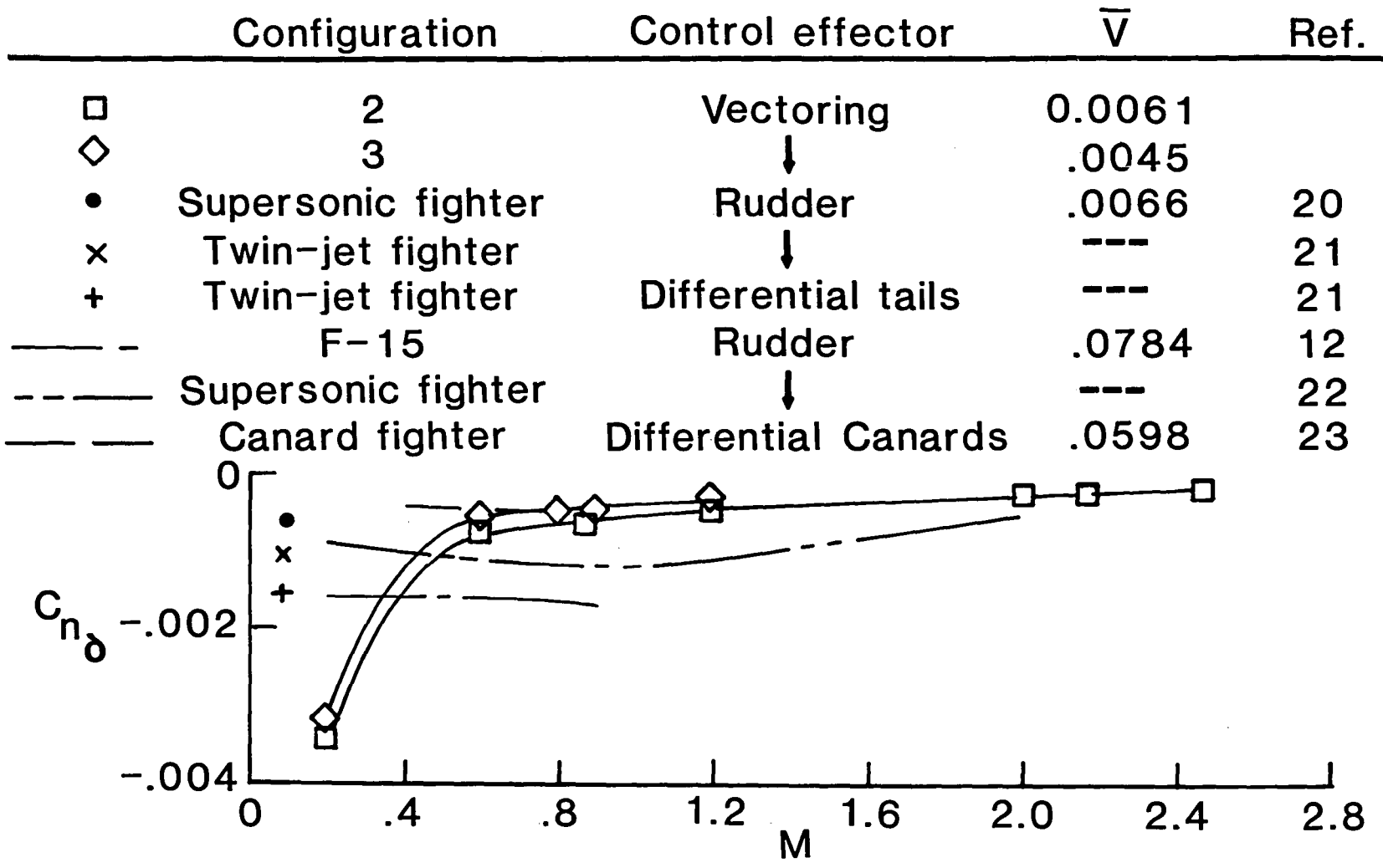

Figure 29.- Variation of directional control power with Mach number, at scheduled NPR $\alpha = 0^{o}$.

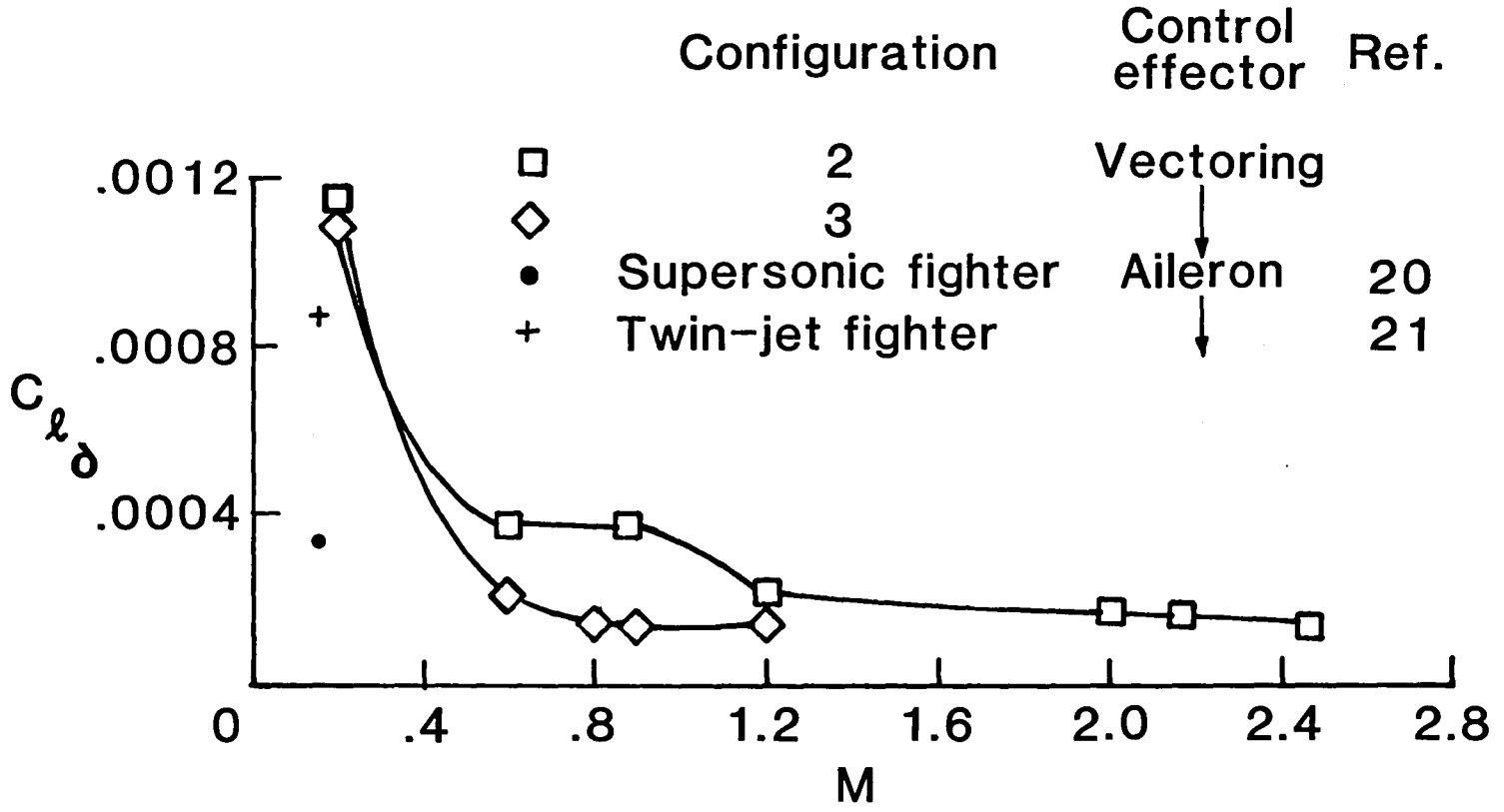

Figure 30.- Variation of lateral control power with Mach number, at scheduled NPR $\alpha = 0^{0}$.

Standard Bibliographic Page

1. Report No.	2. Government Accession No.	3. Recipient's Catalog No.
NASA TM-87741		

4. Title and Subtitle	5. Report Date
MULTIAXIS AIRCRAFT CONTROL POWER FROM THRUST VECTORING AT HIGH ANGLES OF ATTACK	June 1986
	6. Performing Organization Code: 505-62-91-01
7. Author(s): Francis J. Capone and Mary L. Mason	8. Performing Organization Report No.
9. Performing Organization Name and Address: NASA Langley Research Center, Hampton, VA 23665	10. Work Unit No.
	11. Contract or Grant No.
12. Sponsoring Agency Name and Address: National Aeronautics and Space Administration, Washington, DC 20546	13. Type of Report and Period Covered: Technical Memorandum
	14. Sponsoring Agency Code

15. Supplementary Notes

This paper will be presented at the AIAA 4th Applied Aerodynamics Conference June 9-11, 1986, in San Diego, California. AIAA Paper No. 86-1779.

16. Abstract

Extensive research programs conducted at the Langley Research Center have shown that thrust vectoring can be provided by multifunction (nonaxisymmetric) nozzles. Most of this research has been conducted on pitch vectoring at both static and forward flight conditions. Recent efforts have been aimed at evaluating yaw vectoring concepts at static (wind off) conditions. This paper summarizes results for three different twin-engine fighter configurations tested over a Mach number range of 0.15 to 2.47 at angles of attack up to 35°. The objective of these investigations was to determine the multiaxis control power characteristics provided by thrust vectoring. All three configurations employed two-dimensional convergent-divergent nozzles which provided pitch vectoring by differential deflection of the upper and lower nozzle divergent flaps. Three different means of yaw vectoring was tested: (1) a translating nozzle sidewall; (2) yaw flaps located in the nozzle sidewalls; and (3) canted nozzles. These investigations were conducted in the Langley 16-Foot Transonic Tunnel and the Lewis 10x10-Foot Supersonic Tunnel. Longitudinal and direction control power from thrust vectoring was greater than that provided by aerodynamic control effectors at low speed or at high angles of attack.

17. Key Words (Suggested by Authors(s))	18. Distribution Statement
Fighter Aircraft Thrust Vectoring Longitudinal Control Direction Control	Unclassified - Unlimited Subject Category 02

19. Security Classif.(of this report)	20. Security Classif.(of this page)	21. No. of Pages	22. Price
Unclassified	Unclassified	50	A03

For sale by the National Technical Information Service, Springfield, Virginia 22161

End of Document